

# Direct numerical simulation of forced MHD turbulence at low magnetic Reynolds number

By OLEG ZIKANOV AND ANDRE THESS

Center for Physical Fluid Dynamics, Department of Mechanical Engineering,  
Dresden University of Technology, D-01062 Dresden, Germany

(Received 23 May 1997 and in revised form 4 November 1997)

The transformation of initially isotropic turbulent flow of electrically conducting incompressible viscous fluid under the influence of an imposed homogeneous magnetic field is investigated using direct numerical simulation. Under the assumption of large kinetic and small magnetic Reynolds numbers (magnetic Prandtl number  $P_m \ll 1$ ) the quasi-static approximation is applied for the computation of the magnetic field fluctuations. The flow is assumed to be homogeneous and contained in a three-dimensional cubic box with periodic boundary conditions. Large-scale forcing is applied to maintain a statistically steady level of the flow energy. It is found that the pathway traversed by the flow transformation depends decisively on the magnetic interaction parameter (Stuart number). If the magnetic interaction number is small the flow remains three-dimensional and turbulent and no detectable deviation from isotropy is observed. In the case of a strong magnetic field (large magnetic interaction parameter) a rapid transformation to a purely two-dimensional steady state is obtained in agreement with earlier analytical and numerical results for decaying MHD turbulence. At intermediate values of the magnetic interaction parameter the system exhibits intermittent behaviour, characterized by organized quasi-two-dimensional evolution lasting several eddy-turnover times, which is interrupted by strong three-dimensional turbulent bursts. This result implies that the conventional picture of steady angular energy transfer in MHD turbulence must be refined. The spatial structure of the steady two-dimensional final flow obtained in the case of large magnetic interaction parameter is examined. It is found that due to the type of forcing and boundary conditions applied, this state always occurs in the form of a square periodic lattice of alternating vortices occupying the largest possible scale. The stability of this flow to three-dimensional perturbations is analysed using the energy stability method.

---

## 1. Introduction

The suppression of the motion of electrically conducting fluid by a static magnetic field is a subject of increasing interest. In laboratory or industrial flows of liquid metals, where the magnetic Reynolds number is normally very small, the effect of the Lorentz force reduces to Joule dissipation damping three-dimensional motions. The flow becomes essentially independent of the coordinate in the direction of the magnetic field. This phenomenon is of importance for, e.g., construction of effective liquid metal cooling blankets for fusion reactors or for optimization of processes of semiconductor crystal growth or continuous casting of metals (magnetic braking). Numerous applications are also possible connected with the magnetohydrodynamic

control of electrically conducting fluid flows (Gelfgat, Lielausis & Shcherbinin 1975). An example is the MHD drag reduction reviewed by Tsinober (1990).

Being the subject of theoretical (Moffatt 1967; Schumann 1976; Alemany *et al.* 1979; Sommeria & Moreau 1982; Hossain 1991; Davidson 1995, 1997) and numerous experimental (Branover 1978; Votsish & Kolesnikov 1976*a, b*; Kolesnikov & Tsinober 1974; Alemany *et al.* 1979; Eckert 1997, and others) investigations, the evolution of liquid metal turbulent flow in the presence of a static magnetic field is understood to some extent. Joule dissipation is highly anisotropic. Only velocity modes with non-zero gradient in the direction of the magnetic field  $\mathbf{B}_0$  are dissipated. The rate of dissipation is proportional to  $\cos^2\theta$ , where  $\theta$  is the angle between  $\mathbf{B}_0$  and the wavenumber vector  $\mathbf{k}$ . Velocity gradients in the direction of  $\mathbf{B}_0$  are damped and vortical structures are elongated in this direction. The process can also be described as the propagation of momentum and vorticity along the magnetic field lines. The flow becomes anisotropic, the energy being concentrated in the modes independent of the coordinate in the direction of  $\mathbf{B}_0$ . This leads in turn to a decrease of total Joule dissipation. The tendency to anisotropy is opposed by the nonlinear angular energy transfer from modes perpendicular to  $\mathbf{B}_0$  to the other modes which tends to restore isotropy. The balance between Joule dissipation and nonlinear angular energy transfer is decisive for the type of anisotropic flow developing. The ratio between these two terms is estimated by the so-called magnetic interaction parameter (or Stuart number)  $N$ . If  $N$  is large the flow can become two-dimensional in the sense that the velocity field is independent of the coordinate parallel to  $\mathbf{B}_0$ . Both magnetic dissipation and nonlinear angular transfer vanish as the flow approaches this two-dimensional state.

MHD turbulent flows at higher magnetic Reynolds number, which find applications in many astro- and geophysical problems, also demonstrate the development of anisotropy under the action of an imposed constant magnetic field. Among the work in this active area of study we mention that of Oughton, Priest & Matthaeus (1994) where a numerical simulation of decaying MHD turbulence at unit magnetic Prandtl number was performed. A comparison between our results and those of Oughton *et al.* is provided in the concluding section.

One additional remark is necessary concerning the possible comparison of turbulent flow at small magnetic Reynolds number and turbulent flows in stratified and rotating systems (see e.g. Staquet & Sommeria 1996 and Cambon, Mansour & Godeferd 1997 for a review and Hossain 1991, 1994 for demonstration of the similar effect of rotation and magnetic field on homogeneous turbulence). Both stratification and rotation can lead to anisotropy and transition to slow large-scale two-dimensional flow, as a magnetic field does, but the mechanism of the process is fundamentally different. In flows with rotation and stratification disturbances propagate as internal waves and kinetic energy does not change. By contrast, Lorentz force is dissipative, it does destroy kinetic energy of the flow and disturbances are propagated via pseudo-diffusion along magnetic field lines.

It was also shown in previous works that the effect of rigid walls with specific MHD boundary layers is very important. In particular, insulating boundaries normal to the magnetic field introduce the so-called Hartmann effect. It manifests itself as change of mean velocity profile and the formation of thin Hartmann layers at the walls. It is obvious that in such a configuration the flow cannot become purely two-dimensional. In this paper we consider the simplest (and numerically tractable) problem of locally homogeneous flow in a periodic three-dimensional box. It allows us to neglect the influence of walls and focus on the 'pure' process of MHD suppression of turbulence.

A work closely related to the present investigation is the experimental study by Alemany *et al.* (1979), where the decay of turbulent motion of mercury in a homogeneous magnetic field was investigated. The turbulence was generated by a grid moving in a channel. Magnetic field lines were directed along the channel walls. Observations provided a  $t^{-1.7}$  law for decay of the flow energy and a  $k^{-3}$  kinetic energy spectrum. A theoretical explanation based on the balance between Joule dissipation and nonlinear angular energy transfer (and not on the transition to two-dimensionality) was provided. Tsinober (1990) proposed another experimental setup in which the effect of rigid walls is strongly reduced. The flow through a channel with annular cross-section is subjected to a magnetic field in the azimuthal direction. The walls normal to magnetic field and, correspondingly, Hartmann layers are absent in such a configuration.

Suppression of homogeneous turbulence by a magnetic field was treated analytically by Moffatt (1967), Sommeria & Moreau (1982), and Davidson (1995, 1997). Moffatt investigated the case of a strong magnetic field (magnetic interaction parameter  $N \gg 1$ ) and neglected nonlinear energy transfer. It was shown that the flow becomes rapidly two-dimensional (in the sense that velocity is independent of the coordinate in the direction of the magnetic field). At the same time, the energy of the parallel velocity component grows.

Sommeria & Moreau (1982) considered the process of elongation of large-scale vortical structures along the magnetic field. They attributed it to the process of electromagnetic diffusion of vorticity along the magnetic field lines. The effect of Hartmann boundary layers at the insulating walls perpendicular to the magnetic field was also considered. In the limits  $N \gg 1$ ,  $Re \gg 1$  conditions on the typical perpendicular length  $l_{\perp}$  of a vortex were proposed for the flow to be dynamically two-dimensional.

In the work of Davidson (1995, 1997) the basic idea was that the component  $H_{\parallel}$  of global angular momentum parallel to the magnetic field is not affected by the Lorentz force. If mechanical forces do not act on  $H_{\parallel}$  and viscous dissipation is neglected, it can be rigorously demonstrated that  $H_{\parallel}$  is a conserved quantity that imposes strong constraints on the evolution of the flow. In particular, the kinetic energy  $E$  cannot then be fully destroyed. Elongation of the flow structures along the magnetic field lines leads to a continuous decay of Joule dissipation, and the flow eventually takes a two-dimensional form not affected by the magnetic field.

Although it has been studied extensively theoretically and experimentally, the problem of MHD turbulence at low magnetic Reynolds number has received only limited numerical treatment. Among the few existing works we mention those by Shimomura (1991), Cuevas, Ramos & Picologlou (1996) and Cuevas *et al.* (1997*a, b*), where channel flow with a transverse magnetic field was considered, and by Schumann (1976) and Hossain (1991). The last two papers are of most interest for us since homogeneous turbulent flow in a periodic box was studied. Decaying turbulence (in the work of Schumann) and turbulence forced in the wavenumber band  $10 \leq k^2 \leq 13$  (Hossain) were the subjects of direct numerical simulation with the resolution  $32^3$ . In spite of the low resolution and small Reynolds numbers stemming from the low computational power available at the time, certain of the results of Schumann and Hossain are confirmed by our calculations.

The aim of the present work is to understand the long-time evolution of initially isotropic homogeneous forced turbulent flow under the influence of imposed homogeneous magnetic field. Parameters of the problem and governing equations are given in the next section. Numerical experiments performed and computational method are

described in §3. Results of the calculations are given in §§4, 5 and 6, and a short discussion is provided in §7.

## 2. Governing equations

We consider the turbulent motion of an electrically conducting incompressible viscous fluid (e.g. liquid metal). The flow is assumed to be homogeneous and contained in a cubic box of side length  $2\pi$  with periodic boundary conditions. We assume also that there can be a uniform magnetic field  $\mathbf{B}_0$  imposed in vertical direction.

Let the root-mean-square velocity be  $u$ , integral length scale be  $L$ , and magnetic diffusivity be  $\eta$  ( $\eta = (\sigma\mu_0)^{-1}$ ,  $\sigma$  is the electrical conductivity and  $\mu_0$  is the magnetic permeability). The dimensionless parameter

$$Re_m \equiv uL/\eta$$

is known as the magnetic Reynolds number. We suppose that

$$Re_m \ll 1,$$

while the hydrodynamic Reynolds number

$$Re \equiv uL/\nu \gg 1.$$

This assumption is valid for most laboratory and technical flows of liquid metals since the magnetic Prandtl number

$$P_m \equiv \nu/\eta = Re_m/Re$$

is usually very small ( $\sim 10^{-5}$  for sodium and  $\sim 10^{-7}$  for mercury).

If the magnetic Reynolds number is small (in other words the magnetic diffusion time is much smaller than other time scales), the fluctuations  $\mathbf{b}$  of the magnetic field  $\mathbf{B}_0 + \mathbf{b}$  due to fluid motion are much smaller than the applied magnetic field. Moreover, the fluctuation  $\mathbf{b}$ , which determines the induced electric current

$$\mathbf{j} = \mu_0^{-1} \nabla \times \mathbf{b}$$

and the Lorentz force

$$\mathbf{F} = \mathbf{j} \times (\mathbf{B}_0 + \mathbf{b}) \approx \mu_0^{-1} (\nabla \times \mathbf{b}) \times \mathbf{B}_0,$$

adjusts instantaneously to the time-dependence of the velocity. As a result (see e.g. Roberts 1967; Moreau 1990), the quasi-static approximation

$$\eta \Delta \mathbf{b} + (\mathbf{B}_0 \cdot \nabla) \mathbf{u} = 0, \quad \nabla \cdot \mathbf{b} = 0$$

can be used instead of the full magnetic field equation to compute the Lorentz force. After elimination of current density and inclusion of the potential part of the Lorentz force in a modified pressure term, the electromagnetic effect reduces to an anisotropic Joule dissipation. The equations of motion are then

$$\frac{\partial}{\partial t} \mathbf{u}(\mathbf{x}, t) + (\mathbf{u} \cdot \nabla) \mathbf{u} = -\frac{1}{\rho} \nabla p + \nu \Delta \mathbf{u} + \mathbf{F}[\mathbf{u}], \quad (2.1)$$

$$\nabla \cdot \mathbf{u} = 0, \quad (2.2)$$

where the rotational part of Lorentz force is a linear functional of the velocity

$$\mathbf{F}[\mathbf{u}] = -\frac{\sigma B_0^2}{\rho} \Delta^{-1} \frac{\partial^2 \mathbf{u}}{\partial z^2}. \quad (2.3)$$

In (2.3),  $\Delta^{-1}$  is an inverse of the Laplacian operator and the  $z$ -coordinate is directed parallel to the magnetic field. The Fourier transform of (2.3) is

$$\hat{F}[\hat{u}] = -\frac{\sigma (\mathbf{B}_0 \cdot \mathbf{k})^2}{\rho k^2} \hat{u}(\mathbf{k}, t) = -\frac{\sigma B_0^2}{\rho} \cos^2 \theta \hat{u}(\mathbf{k}, t), \quad (2.4)$$

where  $\hat{u}(\mathbf{k}, t)$  is the Fourier transform of velocity field, and  $\theta$  the angle between the wavenumber vector  $\mathbf{k}$  and the imposed magnetic field  $\mathbf{B}_0$ . Applying the Fourier transform to (2.1) and (2.2) and  $\text{rot}^2$  operator to (2.1) we obtain the governing equations in Fourier space as

$$\frac{\partial}{\partial t} \hat{u}(\mathbf{k}, t) = -\frac{1}{k^2} [\mathbf{k} \times (\mathbf{k} \times \hat{q}(\mathbf{k}, t))] - \left[ \nu + \frac{\sigma (\mathbf{B}_0 \cdot \mathbf{k})^2}{\rho k^4} \right] k^2 \hat{u}(\mathbf{k}, t), \quad (2.5)$$

$$\mathbf{k} \cdot \hat{u} = 0, \quad (2.6)$$

where  $\hat{q}$  is the Fourier transform of nonlinear interaction term.

It can be easily seen in (2.5), (2.6) that the additional Joule dissipation produced by the magnetic field is a dissipation of a special kind which leads to the inapplicability of standard Kolmogorov phenomenology to MHD turbulence. First, the Joule dissipation acts equally at all scales of the flow, whereas viscous dissipation is proportional to  $k^2$  and its direct effect is important at small scales only. Therefore, phenomenology based on the energy supply at large scales, energy dissipation at small scales, and the inertial range in between is no longer applicable. Second, the Joule dissipation is anisotropic. It depends on the angle  $\theta$  between the wavenumber vector  $\mathbf{k}$  and the magnetic field  $\mathbf{B}_0$ . The dissipation is maximum for modes with  $\mathbf{k} \parallel \mathbf{B}_0$  and zero for modes with  $\mathbf{k} \perp \mathbf{B}_0$ . The magnetic field tends to eliminate velocity gradients in the direction of  $\mathbf{B}_0$  and, thus, to lengthen turbulent eddies in this direction. The characteristic time of this process, the so-called Joule time, is

$$\tau_J \equiv \rho / \sigma B_0^2. \quad (2.7)$$

The Joule damping leads to a kinematically two-dimensional state, where velocity depends only on the coordinates in the plane perpendicular to  $\mathbf{B}_0$ . This tendency to two-dimensionality is opposed by the nonlinear interaction that tends to restore isotropy of the flow. Energy is transferred continually from the modes with  $\mathbf{k} \perp \mathbf{B}_0$  to the other modes. It is to be noted that, as the flow structure approaches a two-dimensional state, this nonlinear energy transfer as well as the total magnetic dissipation decrease because of the reduction of the energy in modes dependent on the vertical coordinate. The ratio of the Joule to the nonlinear term is the so-called magnetic interaction parameter (or Stuart number)

$$N \equiv \sigma B_0^2 L / \rho u.$$

This parameter can be also defined as the ratio of large-eddy turnover time

$$\tau_{lu} \equiv L/u \quad (2.8)$$

to Joule time (2.7).

A final comment is in order on the assumption of small magnetic Reynolds number. The quasi-static approximation leading to the simplified Lorentz force (2.3) constitutes the first-order theory that is obtained from a systematic expansion of the general magnetic field equation in powers of the magnetic Reynolds number. At this order of approximation Alfvén waves, an important characteristic of many

astrophysical MHD problems, exist only in their degenerate form as pseudo-diffusion along magnetic field lines (Davidson 1995). If the theory were extended to second order, the Alfvén waves would reveal their oscillatory character – an approach that is beyond the scope of the present paper.

### 3. Numerical experiments

Equations (2.5) and (2.6) are solved in a three-dimensional cubic box of side  $2\pi$  with periodic boundary conditions to investigate the response of an initially isotropic turbulence to the sudden application of a magnetic field. Different values of the Stuart number  $N$  are used.

During the calculations, the flow is forced in the following manner. After each time step the energy  $E^<$  contained in Fourier modes with  $k < 2.5$  is evaluated. Then, all such modes are multiplied by  $c = (E_0^</E^<)^{1/2}$ , where  $E_0^<$  is a prescribed value. The coefficient  $c$  is always slightly larger than 1 which allows viscous and magnetic dissipations to be compensated. By this means the energy of modes with  $k < 2.5$  is held at a constant level  $E_0^<$  which is chosen to be 0.75 in all runs.

This forcing was chosen since it does not introduce any artificial isotropy or anisotropy into the flow. In particular, the forcing does not prevent the system from attaining a purely two-dimensional state. Energy supply is distributed over largest-scale modes in proportion to the instantaneous values of the energy in these modes. In the case of MHD flows, the role of forcing seems to be more important than for ordinary turbulence. Indeed, the energy supply scales are also subject to Joule dissipation. The influence of the type of forcing on the flow structure is not investigated in detail here.

A standard pseudospectral technique based on the fast Fourier transform is employed. The resolution is  $128^3$  and  $64^3$ . The aliasing errors are not removed, which allows the cost of calculations to be reduced by a factor about 2. (For a discussion of the importance of aliasing errors in pseudospectral methods see Orszag 1972.) The time-stepping technique includes a second-order leap-frog scheme for the nonlinear term and an exponential solution for the linear terms. To suppress the oscillatory instability inherent in leap-frog methods, the solutions at two subsequent time layers are averaged every 20th time step.

As an initial condition we use the isotropic velocity field calculated with the lower resolution  $32^3$ . During the first (6 for  $128^3$  and 11 for  $64^3$ ) turnover times  $\tau_{tu}$  (defined with the values of  $u$  and  $L$  at the end of this period), the magnetic field is absent. This allows us to obtain a developed turbulent flow with a good degree of isotropy. Then, at the moment  $t = t_0$ , the magnetic field is switched on and remains constant till the end of calculations. During this period the value of  $\sigma B_0^2/\rho$  is set to  $N_0 u(t_0)/L(t_0)$ , where  $N_0$  is a prescribed initial magnetic interaction parameter  $N_0 = N(t_0)$ .

The kinematic viscosity  $\nu$  is chosen to be 0.0054 at resolution  $128^3$  and 0.008453 at resolution  $64^3$ . This implies, respectively,  $Re_L \approx 190$  and  $\approx 128$  for isotropic flow at  $t = t_0$ . It is commonly accepted (see e.g. Jimenez *et al.* 1993) that the necessary condition for an appropriate resolution of small scales of isotropic turbulent flow can be formulated as  $K_{max}\eta > 1$ , where  $K_{max} = 64$  (32) is the maximum wavenumber and  $\eta = (\nu^3/\epsilon)^{1/4}$  is the Kolmogorov dissipation scale. The criterion is satisfied in our calculations. At  $t = t_0$ ,  $K_{max}\eta$  is about 1.59 for resolution  $128^3$  and about 1.13 for resolution  $64^3$ . In the presence of a magnetic field at  $t > t_0$  the coefficient  $K_{max}\eta$  is never less than the values above.

During the numerical runs, the following integral characteristics are calculated as indicators of the transformation of flow structure under the influence of the magnetic field.

(i) Total energies

$$E_i = \frac{1}{2} \int_0^\infty u_i^2(k) dk, \quad i = 1, 2, 3 \quad (3.1)$$

contained in  $i$ th velocity components.

(ii) Integral scales in each direction

$$L_i = \frac{\pi}{2E_i} E_i(0), \quad i = 1, 2, 3, \quad (3.2)$$

where  $E_i(k_i)$  is the one-dimensional longitudinal spectrum of the velocity component  $u_i$ , and  $E_i$  in the denominator is defined by (3.1). In isotropic flow all the scales  $L_i$  must be equal to the integral length

$$L = \frac{\pi}{2u^2} \int_0^\infty k^{-1} E(k) dk$$

defined by the three-dimensional spectrum  $E(k)$  (Hinze 1959).

(iii) Total viscous ( $\epsilon$ ) and magnetic ( $\mu$ ) dissipations calculated according to

$$\epsilon = 2\nu \int_0^\infty k^2 E(k) dk, \quad \mu = \frac{\sigma}{\rho} \sum_i \int_k \frac{(\mathbf{B}_0 \cdot \mathbf{k})^2}{k^2} \hat{u}_i(\mathbf{k}) \cdot \hat{u}_i(-\mathbf{k}) dk.$$

(iv) Taylor microscale  $\lambda = (15\nu u^2/\epsilon)^{1/2}$  and Kolmogorov dissipation length  $\eta = (\nu^3/\epsilon)^{1/4}$ .

(v) Parallel, transverse, and Taylor-scale Reynolds numbers

$$Re_\parallel = \frac{u_\parallel L_\parallel}{\nu}, \quad Re_\perp = \frac{u_\perp L_\perp}{\nu}, \quad Re_\lambda = \frac{u\lambda}{\nu}, \quad (3.3)$$

where  $L_\parallel = L_3$ ,  $L_\perp = (L_1 + L_2)/2$  are parallel and transverse integral scales and  $u_\parallel = E_3^{1/2}$ ,  $u_\perp = (E_1^{1/2} + E_2^{1/2})/2$  are mean velocities in the parallel and transverse directions, respectively.

(vi) Parallel and transverse magnetic interaction parameters

$$N_\parallel = \frac{\sigma B_0^2 L_\parallel}{\rho u_\parallel}, \quad N_\perp = \frac{\sigma B_0^2 L_\perp}{\rho u_\perp}. \quad (3.4)$$

(vii) To check the degree of anisotropy we calculate the normalized mean-square velocity gradients in the direction of  $\mathbf{B}_0$

$$G_1 = \frac{\langle (\partial u_2 / \partial z)^2 \rangle}{2 \langle (\partial u_2 / \partial y)^2 \rangle}, \quad G_2 = \frac{2 \langle (\partial u_3 / \partial z)^2 \rangle}{\langle (\partial u_3 / \partial y)^2 \rangle}. \quad (3.5)$$

Both coefficients are equal to unity in isotropic turbulence and decrease to zero under the influence of a magnetic field in the  $z$ -direction.

(viii) Following Schumann (1976) we calculate the skewness coefficients

$$S_i = \frac{1}{35} (15\nu/\epsilon)^{3/2} \int_k \hat{\Gamma}_{ii}(\mathbf{k}) k^2 d\mathbf{k}, \quad (3.6)$$

where

$$\hat{\Gamma}_{ij}(\mathbf{k}) = \hat{q}_i(\mathbf{k}) \hat{u}_j(-\mathbf{k}) + \hat{q}_j(-\mathbf{k}) \hat{u}_i(\mathbf{k})$$

is the tensor of nonlinear inertial energy transfer. In a purely two-dimensional state without forcing the integral enstrophy transfer

$$\sum_i \int_k \hat{r}_{ii}(\mathbf{k}) k^2 d\mathbf{k} \quad (3.7)$$

must be zero, implying zero skewness  $S = \sum_i S_i$ . Therefore, in his calculations of decaying MHD turbulence, Schumann (1976) used  $S$  as an indicator for the proximity to two-dimensionality. In the case of forced flow, the skewness  $S$  can be different from zero even in a purely two-dimensional state. Nevertheless, the coefficient  $S$  is used in our calculations with the same meaning as in the calculations of Schumann since, as is shown below, the two-dimensional state developing under the impact of a strong magnetic field is laminar and  $S = 0$  always.

In addition to the integral characteristics, the two-dimensional energy spectra  $E(k, \theta)$  and  $\mu(k, \theta)$  are calculated. Here  $E(k, \theta)$  and  $\mu(k, \theta)$  stand for the energy and magnetic dissipation in modes with  $|\mathbf{k}| = k$  and angle between  $\mathbf{k}$  and  $\mathbf{B}_0$  equal to  $\theta$ .

To visualize the spatial structure of the flow three- and two-dimensional pictures of vorticity and velocity fields are used below.

#### 4. Large magnetic interaction parameter

In this section, results of the calculations with a strong magnetic field, i.e. with magnetic interaction parameter  $N \gg 1$  are presented. Numerical resolution is  $128^3$  and viscosity  $\nu$  is equal to 0.0054. At  $t < t_0$  the flow without the magnetic field is calculated. This allows us to obtain a developed isotropic turbulent velocity field. At  $t = t_0$  the homogeneous magnetic field with lines parallel to the  $z$ -axis is switched on. The value of  $\sigma B_0^2 / \rho$  is set to  $10u(t_0)/L(t_0)$ , so that the initial magnetic interaction parameter is  $N_0 = 10$ . In this case the characteristic time  $\tau_J$  of Joule dissipation is ten times smaller than the largest eddy turnover time  $\tau_{tu}$ .

##### 4.1. Integral characteristics

Figures 1–4 show the evolution of integral characteristics of the flow. In all the figures hereafter, time is scaled by the Joule time  $\tau_J$ , and the moment  $t_0$ , at which the magnetic field is switched on, is set to zero.

The anisotropy coefficients  $G_1$  and  $G_2$  given by (3.5) are presented in figure 1. In the absence of magnetic field, at  $t < t_0$ , they are close to unity, and the maximum deviation  $|G_i - 1|$  does not exceed 6%. This indicates a good degree of isotropy of the flow (see also figure 2*a, b*). In the presence of a magnetic field,  $G_1$  and  $G_2$  decrease very fast, implying a rapid transformation of the flow into two-dimensional form. One can see in figure 1 that two stages can be isolated in the process of flow transformation. During the first one, lasting from  $t_0$  to approximately  $t_0 + 5\tau_J$ , the decrease of  $G_1$  and  $G_2$  is extremely rapid. This stage can be considered as dominated by the magnetic dissipation which is very strong (see figure 4*b* and discussion below). Magnetic dissipation continually falls due to the decrease of the energy in modes subject to dissipation. The second stage begins at  $t \approx \tau_{tu}$  and lasts till the end of calculations. During this stage, the flow energy is concentrated in modes perpendicular to the magnetic field and the decrease of  $G_1$  and  $G_2$  is much slower.

Integral length scales  $L_i$  and the Taylor microscale  $\lambda$  are shown in figure 2(*a*). At  $t < t_0$  the scales in different directions are approximately equal which serves as one more confirmation of the isotropy of the flow. After introducing the magnetic field,

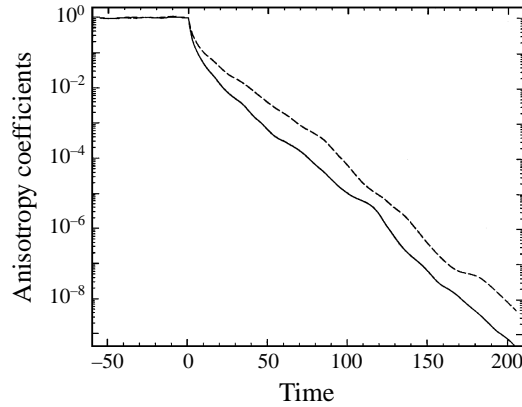


FIGURE 1. Development of anisotropy in three-dimensional MHD flow at high magnetic interaction parameter  $N_0 = 10$ : normalized mean-square velocity gradients  $G_1$  (—) and  $G_2$  (---) (see (3.5)) are shown as functions of time. Scaled time  $(t - t_0)/\tau_J$  is used hereafter in all figures.

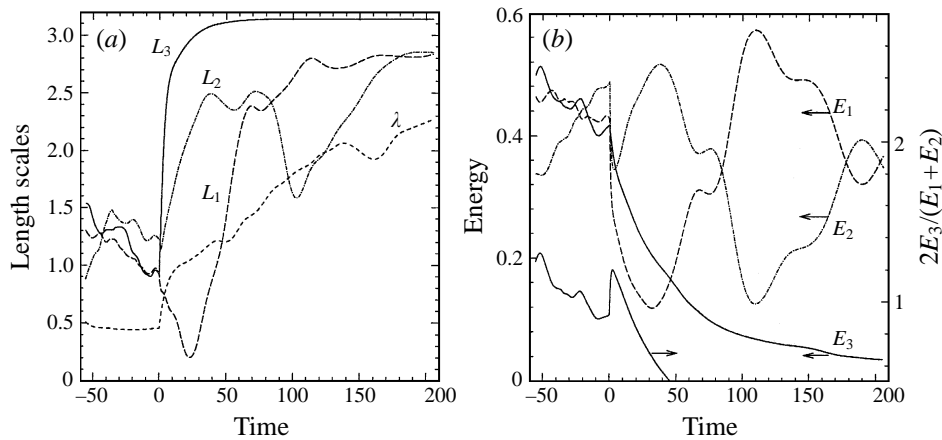


FIGURE 2. Evolution of integral characteristics of the flow at  $N_0 = 10$  (a) Length scales: — — and — · — · —, transverse integral length scales  $L_1$  and  $L_2$ ; —, parallel integral length scale  $L_3$ ; - - - -, Taylor microscale  $\lambda$ . (b) Total energies of velocity components perpendicular  $E_1$  (—),  $E_2$  (— · — · —), and parallel  $E_3$  (—) to the magnetic field. The ratio  $2E_3/(E_1 + E_2)$  between the amplitudes of parallel and transverse motions is also shown.

the parallel scale  $L_3$  begins to grow, the growth rate being very fast during the first stage of magnetic damping introduced above. At  $t > 5\tau_J$  the growth rate falls. By  $t = 50\tau_J$   $L_3$  has nearly reached its maximum possible value  $L_3 = \pi$ . This implies that the flow energy is almost entirely confined to the modes with  $k_3 = 0$  (cf. (3.2)), i.e. to modes perpendicular to the magnetic field.

For the transverse scales  $L_1$  and  $L_2$  one cannot see the initial stage of fast variation. The scales change slowly, the characteristic time being of the order of several turnover times. The curves for  $L_1$  and  $L_2$  demonstrate large instantaneous differences implying a considerable large-scale anisotropy of the flow in a transverse plane. As will be shown below this difference between  $L_1$  and  $L_2$  is a result of the formation of large vortical structures in the flow.

Figure 2(b) presents the time dependence of energies  $E_i$  of different velocity components. One can see that, during the first few Joule times after the application of the

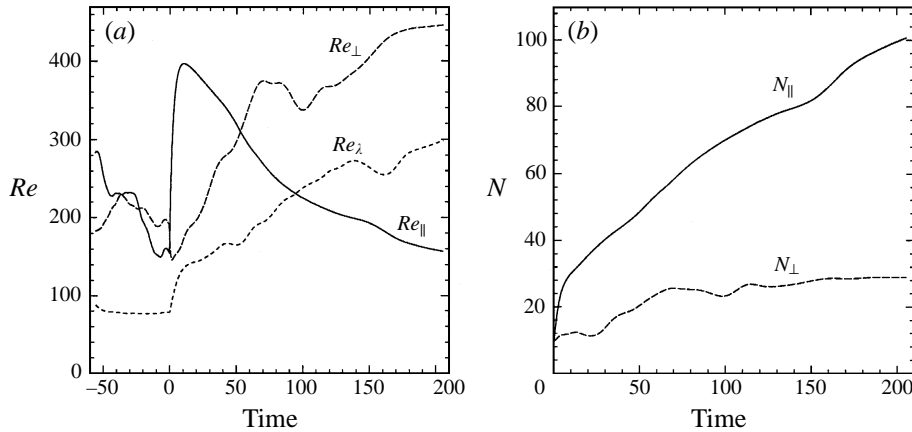


FIGURE 3. Reynolds and Stuart numbers versus time at  $N_0 = 10$ . (a) Parallel ( $Re_{\parallel}$  denoted as —), transverse ( $Re_{\perp}$  denoted as - - -), and Taylor-scale ( $Re_{\lambda}$  denoted as · · · ·) Reynolds numbers. (b) Parallel ( $N_{\parallel}$  denoted as —) and transverse ( $N_{\perp}$  denoted as - - -) Stuart numbers. The curves also show the time dependence of actual eddy turnover time scales in the parallel ( $L_{\parallel}/u_{\parallel}$ ) and transverse ( $L_{\perp}/u_{\perp}$ ) directions.

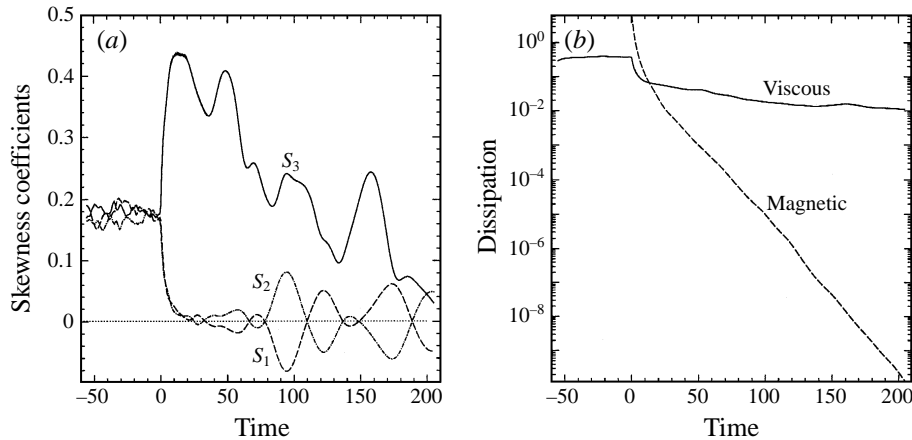


FIGURE 4. Integral characteristics of the flow at  $N_0 = 10$ . (a) Skewness coefficients (3.6): —, parallel coefficient ( $S_3$ ); - - - (· · · ·), transverse coefficients  $S_1$  ( $S_2$ ). (b) Total viscous ( $\epsilon$  denoted as —) and magnetic ( $\mu$  denoted as - - -) dissipation.

magnetic field, the amplitudes of all velocity components decrease. At that time, the ratio  $2E_3/(E_1 + E_2)$  grows. This is in accordance with decay calculations of Schumann (1976) and the linear approximation of Moffatt (1967). The last fact points to the quasi-linear type of evolution at this first stage dominated by the magnetic dissipation.

At the second stage of flow evolution, at  $t > t_0 + 10\tau_J$ , the energy of fluid motion in the direction of the magnetic field falls constantly, whereas the total energy of transverse motions remains at a constant level. The behaviour of transverse velocity components  $u_1$  and  $u_2$  is similar to that of transverse length scales. The energies  $E_1$  and  $E_2$  oscillate slowly, the oscillations being correlated with the oscillations of  $L_1$  and  $L_2$ . Clearly, the reason for both types of oscillations should be the same.

Parallel, transverse, and Taylor-scale Reynolds numbers defined by (3.3) and parallel and transverse Stuart numbers are shown as functions of time in figures 3(a) and 3(b),

respectively. One can see that the values of Reynolds numbers change considerably according to the change of length scales and amplitudes of velocity components. The same is true of the time dependence of parallel and transverse Stuart numbers. The Stuart numbers are proportional to actual parallel and transverse eddy turnover times which can be defined as  $\tau_{tu\parallel} = L_{\parallel}/u_{\parallel}$  and  $\tau_{tu\perp} = L_{\perp}/u_{\perp}$ , respectively (see (3.4)).  $\tau_{tu\parallel}$  and  $\tau_{tu\perp}$  increase with time following the growth of length scales and decrease of the energies of velocity components. Below, we show that this process is associated with the development of large-scale spatial structures in the flow.

The skewness coefficients  $S_i$  given by (3.6) are presented in figure 4(a). At  $t < t_0$ , the  $S_i$  have approximately equal statistically steady values. After introducing the magnetic field, the transverse coefficients  $S_1$  and  $S_2$  fall quickly and, at large time, oscillate near the origin in such a way that their sum is zero. On the other hand, the skewness coefficient in the direction of the magnetic field  $S_3$  grows after the introduction of the magnetic field. During the first few turnover times  $S_3$  compensates the decrease of transverse coefficients so that total skewness  $S$  changes only slightly. Then,  $S_3$  decreases slowly, but remains finite till the end of calculations.

Similar behaviour was observed in low-resolution short-time simulations of freely decaying MHD turbulence by Schumann (1976). For non-forced two-dimensional turbulence the skewness  $S$  must be zero. Therefore, Schumann considered transverse coefficients  $S_1$  and  $S_2$  as behaving in accordance with two-dimensionalization of the flow. On the other hand, the behaviour of  $S_3$  was named anomalous.

In our case of forced flow,  $S$  can be non-zero even in purely two-dimensional flow. But the integral enstrophy transfer (3.7) and, respectively,  $S$  must be zero in a laminar steady flow occupying the largest scale only. Such a state is shown below to be a final state of the flow in the presence of strong magnetic field. Therefore, we can consider  $S$  as a measure for the proximity of the flow to this final state.

The total viscous and magnetic dissipation are shown in figure 4(b). Just after the application of the magnetic field, when the flow is isotropic, magnetic dissipation is very strong. During the first several Joule times  $\mu$  is larger than  $\epsilon$ . As the process of magnetic damping proceeds,  $\mu$  decreases rapidly and, at  $t \approx 13\tau_J$ , becomes smaller than the total viscous dissipation  $\epsilon$ . At large times, when the flow approaches a two-dimensional state, the magnetic dissipation decreases almost exponentially. Another interesting feature, seen in figure 4(b), is the rapid decrease of viscous dissipation  $\epsilon$  during the first stage of magnetic damping. As discussed below, this can be explained by the development of large-scale quasi-two-dimensional structures and corresponding formation of a steeper energy spectrum of the flow.

Two-dimensional energy distributions  $E(k, \theta)$  over wavenumber  $k = |\mathbf{k}|$  and angle  $\theta$  between  $\mathbf{B}_0$  and  $\mathbf{k}$  were calculated using snapshots of the velocity field. The results are partly shown in figure 5(a-d). Figure 5(a) presents energy spectra  $E(k)$  obtained by integration of  $E(k, \theta)$  over  $\theta \in [0, \pi/2]$ . It can be seen that under the influence of the magnetic field the spectrum  $E(k)$  becomes steeper. This tendency is in qualitative agreement with theories of purely two-dimensional turbulence predicting a  $E \sim k^{-3}$  power law (Kraichnan 1967). However, one should be wary of drawing quantitative conclusions from the late-time spectra of figure 5(a), since our two-dimensional flow does not represent fully developed two-dimensional turbulence comparable with that obtained in purely two-dimensional high-resolution simulations (see e.g. Borue 1993). The energy spectrum transformation provides an explanation for the decrease of viscous dissipation demonstrated in figure 4(b). Indeed, one can see that the magnetic field reduces the energy in small-scale modes which are the main participants in the process of viscous dissipation.

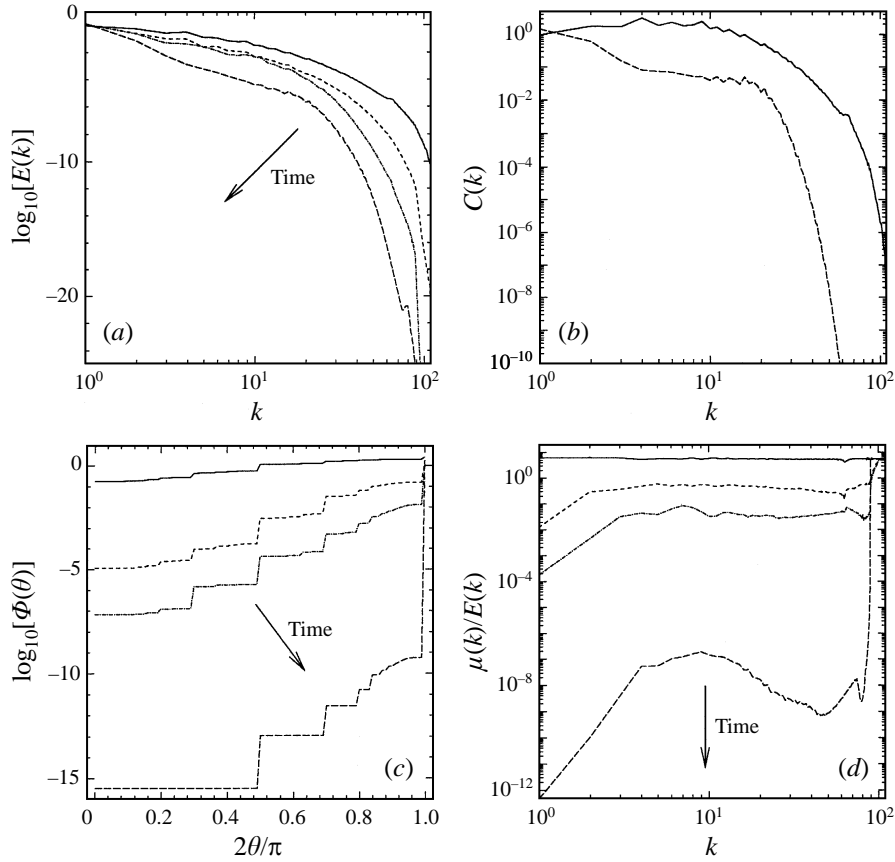


FIGURE 5. Temporal evolution of the flow spectra at high magnetic interaction parameter  $N_0 = 10$ : —,  $t = t_0$ ; - - -,  $t = t_0 + 10\tau_J$ ; - · - · -,  $t = t_0 + 35\tau_J$ ; — — —,  $t = t_0 + 205\tau_J$ . (a) Energy spectrum  $E(k)$ . (b) Compensated energy spectrum  $C(k) = E(k)k^\alpha$ ;  $\alpha = 5/3$  at  $t = t_0$  and  $\alpha = 3$  at  $t = t_0 + 205\tau_J$ . (c) Angular energy distribution  $\Phi(\theta) = \int_0^\theta E(\lambda)d\lambda$ , where  $E(\lambda)$  is the angular spectrum of flow energy. (d) The ratio of Joule dissipation to flow energy  $\mu(k)/E(k)$  as a function of wavenumber  $k$ .

An attempt to find a power-law approximation of energy spectra is presented in figure 5(b). Spectra of the isotropic flow at  $t = t_0$  and the quasi-two-dimensional flow at  $t = t_0 + 205\tau_J$  are compensated by  $k^{5/3}$  and  $k^3$  respectively. Our resolution is too poor to allow any reliable conclusions. At least, for  $4 < k < 12$ , power-law ranges can be seen for both the curves. For quasi-two-dimensional flow, the scaling exponent is clearly smaller than  $-3$  which is typical of the large-scale vortices developed in the flow to this time (see below). Such a scaling was not detected in the earlier simulation of forced homogeneous turbulence in the presence of strong magnetic field performed by Hossain (1991). Instead, the spectrum  $E(k) \sim k^{-3}$  was found at high  $k$  in the flow nearing a kinematically two-dimensional state. The discrepancy can be related to the forcing at  $10 \leq k^2 \leq 13$  used in the work of Hossain which does not allow the structures of largest scale to develop in the flow. The difference in the wavenumber band at which forcing is applied seems to be also responsible for the fact that the inverse energy cascade at small  $k$  found by Hossain was not detected in our calculations.

Alemaný *et al.* (1979) also measured  $k^{-3}$  energy spectra of decaying MHD turbulence but argued that this scaling as well as the  $t^{-2}$  law for energy decay is due to establishing a quasi-steady equilibrium between Joule dissipation and nonlinear transfer in an anisotropic three-dimensional flow.

Figure 5(c) shows the angular energy spectra for different moments of time. Instead of the angular distribution

$$E(\theta) = \int_0^\infty E(k, \theta) dk$$

we use the integral

$$\Phi(\theta) = \int_0^\theta E(\lambda) d\lambda,$$

which gives the total energy of all modes contained in the cone of axis  $\mathbf{B}_0$  and semi-angle  $\theta$ . The jumps of curves in figure 5(c) are due to the finite numerical resolution. A jump occurs when a large-scale energetic mode is taken into account for the first time. In an isotropic flow the distribution of energy over  $\theta$  is homogeneous and  $\Phi(\theta)$  must be a linear function of  $\theta$  (cf. the curve for  $t = t_0$  in figure 5c), while in purely two-dimensional flow the spectrum is  $\Phi = E\delta(\theta - \pi/2)$ . The magnetic field damps quickly all modes except those with wavenumber vectors in the plane perpendicular to  $\mathbf{B}_0$ . At  $t = t_0 + 205\tau_J$ , the energy in modes out of this plane constitutes less than  $10^{-9}$  of the total energy. The flow takes a kinematically quasi-two-dimensional form in which the velocity field is virtually independent of  $z$ .

Two-dimensional spectra  $\mu(k, \theta)$  of Joule dissipation were also computed. To show distributions of  $\mu$  over length scales we use the wavenumber spectra obtained by integration over  $\theta$ . The ratio  $\mu(k)/E(k)$  is shown in figure 5(d) for different  $t$ . It can be easily shown (see e.g. Schumann 1976) that in the isotropic case one must have  $\mu(k)/E(k) = 2/3\tau_J^{-1} = \text{const}$ . The curve for  $t = t_0$  in figure 5(d) agrees well with this condition. The root-mean-square value of  $\mu(k)/E(k)\tau_J$  is equal to  $0.6446 \approx 2/3$ .

Transformation of the velocity field into a kinematically two-dimensional state reduces the total magnetic dissipation but does not strongly change its distribution over  $k$ . One can see in figure 5(d) that except for forced modes at smallest  $k$  and modes at largest  $k$  subject to viscous dissipation, the ratio  $\mu(k)/E(k)$  remains only weakly dependent on  $k$ . This is valid also at large  $t$  when the flow takes essentially a kinematically two-dimensional form. We can state that in the inertial range the relative intensity of Joule dissipation does not depend on the length scale. In other words, the level of anisotropy is approximately equal at all scales in this range.

#### 4.2. Spatial structure of the flow

In this section we look at the evolution of the spatial structure of the flow under the influence of the magnetic field. Three- and two-dimensional plots of vorticity and velocity fields are employed.

The development of the vorticity field during one turnover time after the introduction of the magnetic field is illustrated in figure 6. Vorticity vectors are calculated at all nodal points using fast Fourier transform. Following previous studies of isotropic turbulence at moderate Reynolds number (Vincent & Meneguzzi 1991; Jimenez *et al.* 1993) the regions of vorticity with amplitude above a certain limit are plotted: in figure 6 we draw all vectors  $\mathbf{w}$  satisfying the condition  $|\mathbf{w}| > 3w_{\text{mean}}$ , where  $w_{\text{mean}}$  is a root-mean-square vorticity amplitude.

In isotropic flow at  $t = t_0$  one can see the well-known pattern of localized turbulent structures. Davidson (1997) proposed a description of turbulent decay at large  $N$

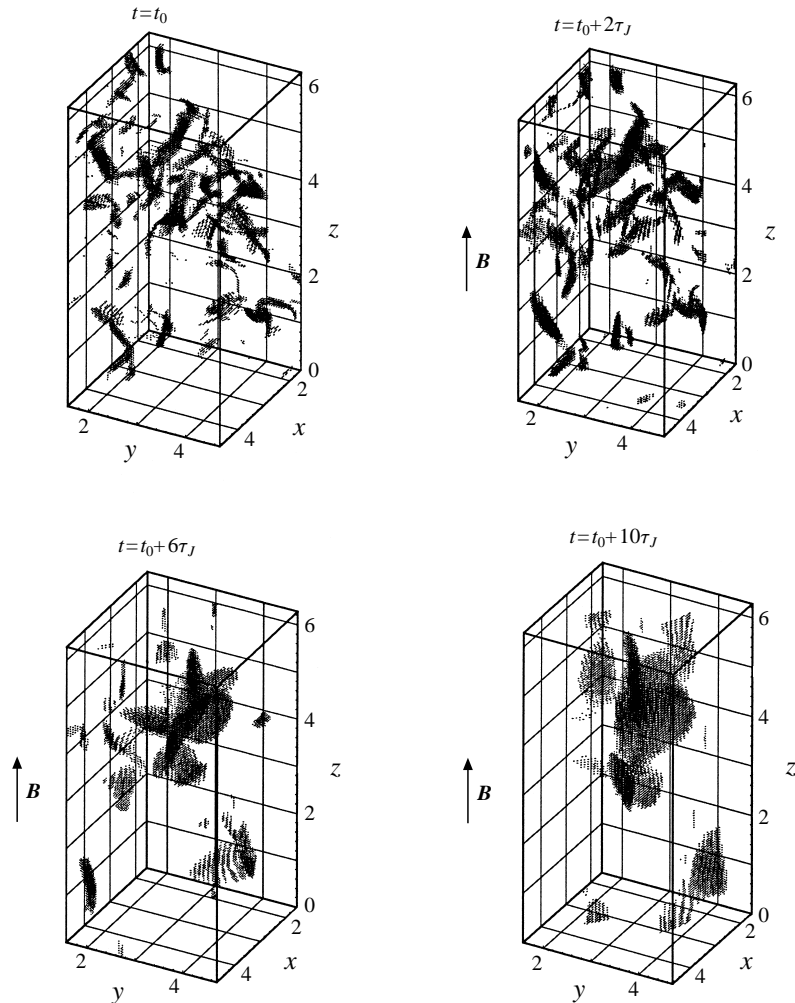


FIGURE 6. Snapshots of vorticity fields at the initial stage  $t \leq t_0 + \tau_{tu}$  of the flow evolution at high magnetic interaction parameter  $N_0 = 10$ : vectors  $\boldsymbol{w}$  with  $|\boldsymbol{w}| > 3w_{mean}$  are plotted. Only the part  $\pi/2 < x < 3\pi/2$ ,  $\pi/2 < y < 3\pi/2$ ,  $0 < z < 2\pi$  of computational box is shown for better resolution.

based on his studies of the evolution of isolated axisymmetric vortices. According to Davidson, vortices parallel to  $\boldsymbol{B}_0$  elongate in the direction of  $\boldsymbol{B}_0$  and form long thin columnar vortex tubes. Vortices transverse to  $\boldsymbol{B}_0$  disintegrate into patterns of sheets oriented along the magnetic field lines. Then, the evolution of the essentially two-dimensional flow is determined by the slow quasi-two-dimensional interaction of sheets and tubes.

Our calculations show that this qualitative picture is true for the evolution of large-scale structures at later stages of flow transformation (see below). The key feature of the initial stage  $t \leq t_0 + \tau_{tu}$  is a merging of small turbulent vortices into large vortical structures. This is seen in figure 6 and is confirmed by the modification of the energy spectrum  $E(k)$  in figure 5(a) and by the drop of total viscous dissipation in figure 4(b). The process of merging is accompanied by rapid growth of anisotropy. The anisotropy is difficult to see in the early velocity fields shown in figure 6. Vortex blobs do not appear strongly elongated in the direction of  $\boldsymbol{B}_0$  even at  $t = t_0 + 10\tau_J$ .

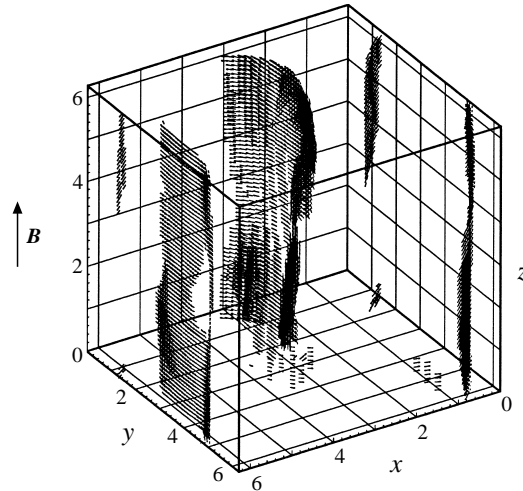


FIGURE 7. Snapshot of vorticity fields at  $t = t_0 + 35\tau_J$  and  $N_0 = 10$ : vorticity vectors  $\boldsymbol{w}$  with  $|\boldsymbol{w}| > 2.5w_{mean}$  are shown.

But the change of angular distribution of flow energy (see figure 5c), decrease of mean velocity gradients  $G_1$  and  $G_2$  in figure 1, and rapid growth of the parallel length scale  $L_3$  in figure 2(a) demonstrate the development of considerable anisotropy of the flow.

The further evolution of the flow can be described as follows. The velocity field becomes virtually independent of  $z$ . The typical vertical length scale takes its maximum possible value (cf. figure 2a) and flow structures extend in the vertical direction over the whole computational box. The flow dynamics is defined by quasi-two-dimensional evolution of the large-scale structures. An example is given in figure 7. One can see that the vorticity field is constituted by large vortex sheets having vertical scale equal to the box side and transverse scale approximately two times smaller. Now we can explain the slow oscillations of transverse integral length scales  $L_1$  and  $L_2$  shown in figure 2(a). The oscillations are associated with the rotation of vortex sheets. At  $t = t_0 + 35\tau_J$ , the sheets are mainly oriented along the  $y$ -axis and, correspondingly,  $L_2$  is large and  $L_1$  is small at this time. At  $t = t_0 + 105\tau_J$ , the vortex sheets are oriented more along the  $x$ -axis (see figure 8) and, correspondingly, the ratio between  $L_1$  and  $L_2$  is reversed. The vertical gradients are almost negligible at  $t = t_0 + 105\tau_J$  and we use in figure 8 the projection of vorticity field on the  $(x, y)$ -plane.

One can note in figure 7 that the component of vorticity in the direction of the magnetic field does not dominate. To check this we calculated the maxima of vorticity components at different moments of time (see figure 9). For a long time (corresponding to the existence of vortex sheets) the vertical component  $w_3$  is of the same order of magnitude as the transverse components  $w_1$  and  $w_2$ . This implies that particle trajectories are helical rather than purely circular structures. As a consequence, mass transport parallel to the magnetic field may well persist even at high values of the magnetic interaction parameter.

We also plotted velocity fields of the flow dominated by vortex sheets. The conclusion is that the sheets are located exactly in the regions with largest horizontal gradients of vertical velocity component. At moderate times, this component is of the same order of magnitude as the transverse components (cf. figure 2b).

The decrease of vertical velocity with time is accompanied by instability and rolling up of vortex sheets. This results in the development of new large-scale vortical

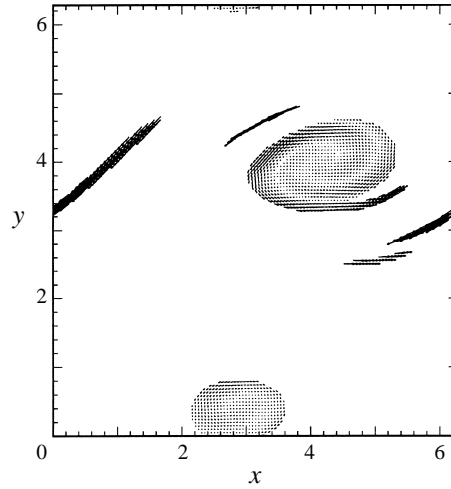


FIGURE 8. Flow structure at  $t = t_0 + 105\tau_J$  and  $N_0 = 10$ . Projection  $(w_1, w_2)(x, y)$  with  $|w| > 2w_{mean}$  on the plane  $z = \pi$  is shown.

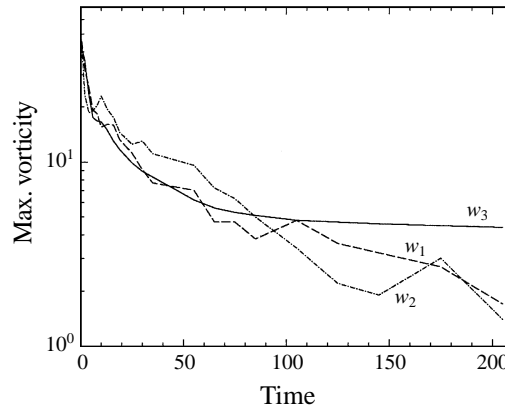


FIGURE 9. Largest values of vorticity component as functions of time at  $N_0 = 10$ .  
 — —,  $w_1$ ; - · - · -,  $w_2$ ; — —,  $w_3$ .

structures – vortex columns with strong vertical vorticity. An illustration is given in figure 8. Vortex columns and sheets coexist for a rather long time, columns becoming more and more pronounced. Accordingly, vertical velocity and transverse vorticity components fall with time, whereas transverse velocity and vertical vorticity remain approximately constant. By the time  $t = t_0 + 205\tau_J$ , which is the final point of our three-dimensional calculations, the maximum  $w_3$  is three times larger than the maximum  $w_1$  and  $w_2$ .

The final flow obtained in three-dimensional calculations is presented in figure 10. We plot the projection  $(u_1, u_2)(x, y)$  of the velocity field on the plane  $z = \pi$ . Filled contours of the absolute value of vertical vorticity component  $|w_3|$  in the same plane are also given. One can see that vortex sheets are not seen any more. Instead, two large vertical counter-rotating vortices define the flow dynamics. The flow pattern is strikingly similar to that obtained in earlier calculations by Hossain (1991). The development of two quasi-two-dimensional large-scale vortices seems to be a natural

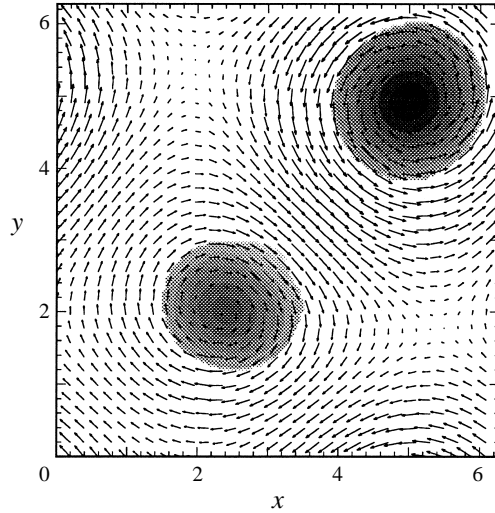


FIGURE 10. Final state of forced MHD turbulence obtained in three-dimensional calculations with high magnetic interaction parameter  $N_0 = 10$ : flow structure at  $t = t_0 + 205\tau_J$  is shown using projection  $(u_1, u_2)(x, y)$  of velocity field on the plane  $z = \pi$  and filled contours of absolute value of vertical vorticity component  $|w_3|$  with  $|w| > 2w_{mean}$ .

response of the system to the applied strong magnetic field consistent with boundary conditions and forcing (see also the discussion in the next section).

#### 4.3. Final two-dimensional state

Calculations with large magnetic interaction parameter discussed above show a rapid transformation of an initially isotropic three-dimensional flow into a kinematically quasi-two-dimensional form. Here we understand two-dimensionality in the sense that the velocity does not depend on the coordinate in the direction of the magnetic field. The mean velocity gradients  $G_1$  and  $G_2$  go exponentially to zero (figure 1). The flow energy is concentrated in the Fourier modes with wavenumber vectors normal to the lines of magnetic field (figure 5c). In accordance, the total magnetic dissipation vanishes (figure 4b). The flow takes the form of two large columnar vortices, their inherent instability being obviously suppressed by the Lorentz force.

A natural question arises in connection with these results. How close is the flow obtained in three-dimensional calculations to true two-dimensional flow? Note that our idealized formulation does not forbid purely two-dimensional states.

To be more precise we reformulate the question in the following manner:

(i) To what accuracy can the flow at large time be described by two-dimensional Navier–Stokes equations?

(ii) Is there a final steady state? If yes, is this state an exact solution of two-dimensional equations?

To answer the questions we performed a simple numerical experiment. The numerical code was adapted to the purely two-dimensional case when all variables are independent of the coordinate  $z$  in the direction of the magnetic field. In this case the Lorentz force drops out. Viscosity  $\nu$ , numerical resolution, and forcing remained the same as in three-dimensional calculations. As an initial condition we used the velocity field obtained at  $t = t_0 + 75\tau_J$ , i.e. when the flow is kinematically two-dimensional

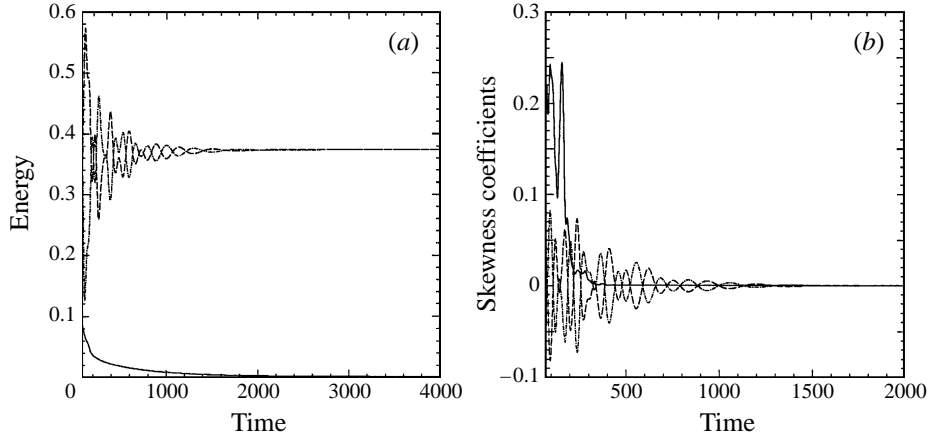


FIGURE 11. Two-dimensional calculations. (a) Total energies of velocity components perpendicular  $E_1$  (—),  $E_2$  (- · - · -), and parallel  $E_3$  (— · —) to the magnetic field versus time. (b) Skewness coefficients (3.6) versus time: —, parallel coefficient ( $S_3$ ); — · — (- · - · -), transverse coefficients  $S_1$  ( $S_2$ ).

with a good degree of approximation. All the Fourier modes except those with the wavenumber vectors normal to the magnetic field were cut off.

A comparison between two-dimensional and three-dimensional calculations has revealed that the computed characteristics of the flow (length scales, amplitudes of velocity components, skewness coefficients, etc.) coincide with good accuracy till the final point  $t = t_0 + 205\tau_J$  of the three-dimensional run. Thus, we can state that the solution obtained at late stages of three-dimensional calculations can be reproduced by a purely two-dimensional numerical code. Inevitable angular energy transfer is counterbalanced by Joule dissipation. At large magnetic interaction parameter  $N_0 = 10$ , this competition leads to almost absolute cancellation of all non-two-dimensional processes and the flow dynamics is well described by the two-dimensional Navier–Stokes equations.

In an attempt to find a final steady state we produced two-dimensional solutions beyond the point  $t = t_0 + 205\tau_J$ . Flow evolution is rather slow in this case. It is determined by the development of two counter-rotating vortices shown in figure 10. As an illustration, figure 11(a, b) presents total energies  $E_i$  and skewness coefficients  $S_i$  ( $i = 1, 2, 3$ ) as functions of time. One can see that after approximately  $t = t_0 + 500\tau_J$ , the skewness coefficient  $S_3$  goes to zero implying the vanishing integral enstrophy transfer inherent in two-dimensional laminar flows.

It can be seen in figure 11(a) that at  $t \rightarrow \infty$  amplitudes of velocity components approach definite limiting values. We performed computations till  $t = t_0 + 12500\tau_J$  and found that after  $t \approx t_0 + 8000\tau_J$  velocity field did not change anymore. The energy concentrates in the modes of largest scale and the final steady flow has the strikingly simple form of Kolmogorov-like square cellular flow (see e.g. Meshalkin & Sinai 1961; Gotoh & Yamada 1986):

$$u = b \sin y, \quad v = a \sin x, \quad w = c \cos x - bc/a \cos y, \quad (4.1)$$

where

$$a = 1.2131, \quad b = 1.2020, \quad c = 0.20239.$$

When writing (4.1) we used the spatial periodicity of the flow and made shifts in

$(x, y)$ -space to eliminate constant phases. Amplitudes of the Fourier modes other than (4.1) decrease continually and are smaller than  $10^{-6}$  at  $t = t_0 + 12500\tau_J$ .

Now we can give a positive answer to question (ii) above. The steady final state exists and it is purely two-dimensional. One can easily check that (4.1) is an exact solution of the two-dimensional Navier–Stokes equations with our forcing at any  $a$ ,  $b$ , and  $c$ . The only condition to be satisfied is

$$a^2 + b^2 + c^2(1 + b^2/a^2) = 4E_0,$$

where  $E_0$  is the total energy in the large-scale modes prescribed by the forcing. In additional calculations with resolution  $64^3$  and  $32^3$  and magnetic interaction number  $N_0 = 0.5, 0.815,$  and  $0.85$  the final steady two-dimensional solutions of the kind (4.1) were always obtained. The specific values of constants  $a$ ,  $b$ , and  $c$ , however, were found to depend on the parameters of the problem and initial conditions.

It is obvious that the evolution into a laminar steady flow is conditioned by the value of the Reynolds number, boundary conditions, and forcing used in this study. It is likely that a state of two-dimensional turbulence with irregular spatio-temporal dynamics would be attained if the simulations were performed at higher  $Re$  or excitations with wavelength larger than  $2\pi$  were allowed. The special form (4.1) of final laminar flow is very similar to vortical final states of freely decaying two-dimensional turbulence predicted by the selective decay, ‘sinh-Poisson’ equation, or maximum entropy theories (see e.g. Matthaeus *et al.* 1991; Montgomery *et al.* 1992; Robert & Sommeria 1991). In the case of periodic boundary conditions an initially irregular turbulent two-dimensional flow was found to relax to the coherent structure of two counter-rotating vortices with nearly circular cross-section located in such a way as to maximize their separation distance. The flow (4.1) obviously belongs to this class of solutions. However, when assuming the relevance of the theories mentioned above to our results one should be aware that the selective decay process implies freely decaying turbulence and an inverse energy cascade to largest scales, whereas our calculations are for forced flow and an inverse cascade was not detected. The observation of such coherent structures in our simulations is probably due to the fact that the dissipation (and forcing) are weak in the two-dimensional state, and the flow is dominating by inertia.

Our calculations are performed for a highly idealized system and we can only suppose that the results reflect some general properties of real MHD flows. There are experimental indications (for a review see e.g. Tsinober 1990) that a magnetic field leads to a quasi-two-dimensional flow and reduces strongly the intensity of turbulent fluctuations. It was observed that in such flows the velocity component parallel to the magnetic field is far from being zero. This phenomenon is well reproduced by our calculations. In the case  $N_0 = 10$ , a finite albeit small value of  $c$  was obtained. In another run, with  $N_0 = 0.85$  and resolution  $32^3$ , the parallel velocity component was larger than the transverse ones.

The presence of fluid motion in the direction of the magnetic field becomes especially interesting if we consider the problem of passive scalar transfer. This problem can be of interest if one deals, for example, with Rayleigh–Bénard convection under an external magnetic field. This type of convection appears in astro- and geophysical systems. The limit of low magnetic Reynolds number employed here is applicable to such flows if one considers the motions at small scales. Clearly non-zero velocity in the direction of the magnetic field is of importance in this case since it can transfer heat even when all velocity fluctuations are suppressed.

## 4.4. Stability analysis

Calculations with low magnetic interaction number discussed in the next section confirm the intuitively obvious fact that Kolmogorov cellular flow (4.1) presents an attractor only in a certain part of  $(N, Re)$ -plane. Outside this region, the flow remains three-dimensional and chaotic. In an attempt to find the boundary of the basin of this attractor we performed the stability analysis. The linear and energy stability of (4.1) to three-dimensional perturbations in the presence of a magnetic field were examined. The procedure is given in detail in the Appendix. Now we discuss the formulation and results briefly.

We consider (4.1) as a basic flow maintained by the forcing and look for the critical Reynolds number  $Re_c(N)$  such that at  $Re < Re_c$  or  $Re > Re_c$  the flow is correspondingly stable or unstable in the sense of linear or energy stability. The Reynolds and Stuart numbers should be defined with typical length and velocity scales of flow (4.1) which are

$$u = (2/3E_0)^{1/2}, \quad L = \pi$$

for any set of  $a$ ,  $b$ , and  $c$ . These scales differ strongly from the scales  $u(t_0)$ ,  $L(t_0)$  used for the definition of  $Re$  and  $N$  in the full calculations (the consequences are seen in figure 3*a, b*). To allow comparisons of stability limits and the results of three-dimensional runs we will use reciprocal viscosity  $\nu^{-1}$  and reciprocal Joule time  $\tau_J^{-1} = B_0^2 \sigma / \rho$  instead of  $Re$  and  $N$ .

The solution (4.1) includes a whole family of flows with different  $a$ ,  $b$ , and  $c$ . Well-known members of the family are the classical Kolmogorov flow  $a \neq 0$ ,  $b = c = 0$  (see e.g. Meshalkin & Sinai 1961) and square cellular flow  $a = b \neq 0$ ,  $c = 0$  (Gotoh & Yamada 1986; Thess 1992). Since we are interested in the most stable solutions the critical parameter  $\nu^{-1}$  should be maximized over  $a$ ,  $b$ , and  $c$ .

Meshalkin & Sinai (1961) have shown in their pioneering paper that Kolmogorov flow is most unstable to infinitely long-wave perturbations. Later, this kind of wave was shown to be most dangerous for other periodic cellular flows. Our aim here is not to examine the stability of (4.1) itself but to understand the results of three-dimensional runs where the maximum allowed wavelength is  $2\pi$ . Therefore, when solving stability problem, we restrict our consideration to perturbations compatible with periodic boundary conditions, that is to the perturbations with integer wavenumber  $k_i$ . Moreover, since the transition between two-dimensional and three-dimensional states is of interest for us, only three-dimensional perturbations are considered.

It is shown in the Appendix that linear stability analysis does not explain the results of nonlinear calculations. The one-dimensional basic solutions (4.1) with  $b = 0$  are linearly stable at any values of  $\tau_J^{-1}$  and  $\nu^{-1}$  to perturbations with integer wavenumbers. The main results of energy stability calculations are presented in figure 12. At zero magnetic field the stability limit is  $\nu^{-1} = 3.825$ , the most stable configuration of the basic flow being that with  $u = v = 0$ ,  $w = (2E_0)^{1/2}(\cos x + \cos y)$ . The magnetic field acts as a source of additional dissipation of the perturbations. In accordance, the critical  $\nu^{-1}$  grows with  $\tau_J^{-1}$ . At  $\tau_J^{-1} > 0.5$ , the one-dimensional basic flow with  $b = 0$  becomes most stable. One can see in figure 12 that the energy stability threshold grows significantly with the strength of the magnetic field. At large  $\tau_J^{-1}$  the dependence is approximately linear.

The energy stability curve is compared in figure 12 with the results of full three-dimensional calculations. In the  $(\tau_J^{-1}, \nu^{-1})$ -plane we denote the points where the transition from isotropic turbulent flow to (4.1) is observed and the points where the

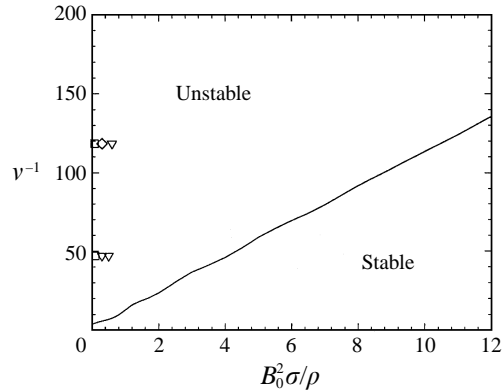


FIGURE 12. Results of energy stability calculations. —, Limit of energy stability of cellular flow (4.1) to three-dimensional perturbations as a function of  $\tau_J^{-1} = B_0^2 \sigma / \rho$ . Stability limits are maximized over constants  $a$ ,  $b$ , and  $c$  of the basic flow.  $\nabla$  ( $\square$ ) denote the points where transition from isotropic turbulent flow to cellular flow (4.1) was observed (was not observed) in full three-dimensional calculations. Symbol  $\diamond$  denotes the point where intermittent three-/two-dimensional behaviour was detected (see §6).

flow remains three-dimensional and turbulent. Also, as discussed in §6, one run gives a kind of intermittent two/three-dimensional behaviour. One can see that suppression of three-dimensional fluctuations and transition to Kolmogorov flow (4.1) occur at much smaller  $\tau_J^{-1}$  (much larger  $\nu^{-1}$ ) than required by the energy stability theory.

### 5. Small magnetic interaction parameter

In this section we discuss the transformation of an initially isotropic turbulent flow under the impact of weak magnetic fields. The run was performed with magnetic interaction parameter  $N(t_0) = 0.1$ . Such a small value of  $N_0$  implies a large typical time  $\tau_J$  of Joule dissipation and, correspondingly, slow mean evolution of the flow. A long-time run is required to see this evolution. The current level of computational power does not allow such a run to be performed with 128 trial functions in each direction as for the case  $N_0 = 10$ . Therefore, calculations were carried out with lower resolution  $64^3$ . The kinematic viscosity  $\nu$  was set to 0.08453. This corresponds to a Reynolds number at  $t = t_0$  equal to 128.

Integral characteristics of the flow are shown as functions of time in figure 13(a, b). As before, time is scaled by the Joule dissipation time  $\tau_J$  and the moment  $t_0$  of application of the magnetic field is set to zero. It must be noted that the time unit in figure 13(a, b) is much larger than in figures 1–4. It is now 10 eddy turnover times  $\tau_{tu}$ .

Among the computed integral characteristics, normalized mean-square velocity gradients  $G_1$  and  $G_2$  (figure 13a) and energies  $E_i$  of velocity components (figure 13b) are chosen to be shown. One can not see any change of statistical behaviour of these quantities with time. The mean values and levels of fluctuations remain approximately the same. Similar pictures were observed for other integral characteristics of the flow, such as length scales  $L_i$ , skewness coefficients  $S_i$ , and total viscous and magnetic dissipations  $\epsilon$ , and  $\mu$ . The energy spectra  $E(k)$  are virtually unchanged in the presence of a weak magnetic field in comparison with the non-magnetic case. We can conclude that the transformation of the flow into the laminar two-dimensional form described in the previous section does not occur at such a small  $N$ . The flow remains turbulent and three-dimensional. As an illustration, figure 14 shows the structure of the vorticity

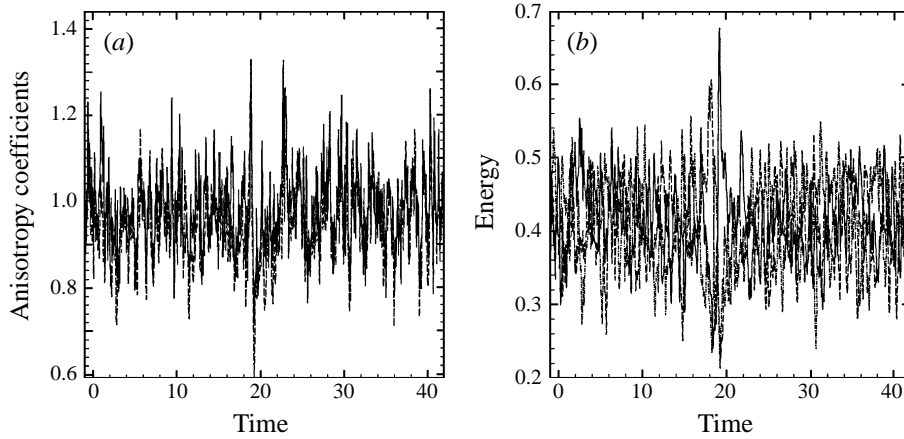


FIGURE 13. Evolution of integral characteristics of the flow at low magnetic interaction parameter  $N_0 = 0.1$  (cf. figures 1 and 2b for comparison with the strongly anisotropic case). (a) Normalized mean-square velocity gradients  $G_1$  (—) and  $G_2$  (---) (see (3.5)). (b) Total energies of velocity components  $E_1$  (—),  $E_2$  (- · - · -), and  $E_3$  (····).

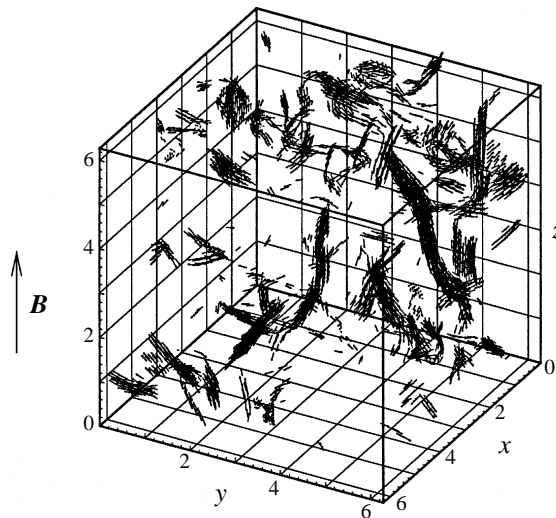


FIGURE 14. Snapshot of vorticity fields at  $t = t_0 + 42\tau_J$  as an example of the flow structure at low magnetic interaction parameter  $N_0 = 0.1$ . Vorticity vectors  $w$  with  $|w| > 2.5w_{mean}$  are shown.

field at  $t = t_0 + 42\tau_J$ . A pattern of localized vortical structures typical of ordinary Navier–Stokes turbulence can be seen.

An important question to be discussed concerns the possible deviation of the flow structure from isotropy. Here we can consider isotropy only in a statistical sense because of permanent chaotic deviations from this state due to the fluctuations of energy-containing modes. The anisotropy coefficients  $G_1$  and  $G_2$  in figure 13(a) seem to have mean values smaller than 1. To quantify this deviation we calculated root-mean-squares of  $G_1$  and  $G_2$  at  $t_0 + 5\tau_J < t < t_0 + 42\tau_J$  and obtained 0.984 for  $G_1$  and 0.952 for  $G_2$ . Also, the total magnetic dissipation  $\mu$  remains at the statistically constant level, whereas  $\mu$  must fall if an angular redistribution of energy occurs. We can conclude that deviation from isotropy, if present, is very small. The flow remains

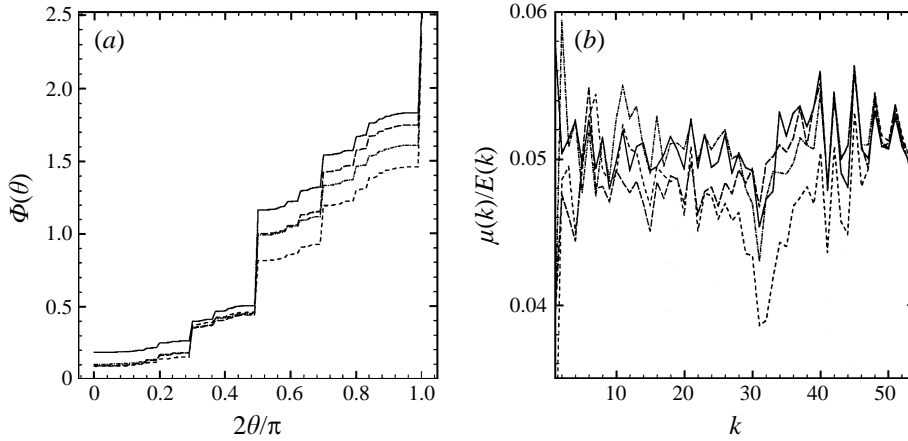


FIGURE 15. Temporal evolution of flow spectra at low magnetic interaction parameter  $N_0 = 0.1$  (cf. figure 5c, d): —,  $t = t_0$ ; - - -,  $t = t_0 + 11.2\tau_J$ ; - · - · -,  $t = t_0 + 26.6\tau_J$ ; — — —,  $t = t_0 + 42\tau_J$ . (a) Angular energy distribution  $\Phi(\theta) = \int_0^\theta E(\lambda)d\lambda$ , where  $E(\lambda)$  is the angular spectrum of flow energy. (b) The ratio of Joule dissipation to flow energy  $\mu(k)/E(k)$  as a function of wavenumber  $k$ .

approximately isotropic. This conclusion is confirmed by the angular energy spectra presented in figure 15(a). Curves for  $t > t_0$  are very close to the curve at  $t = t_0$  corresponding to the initial quasi-isotropic state. (Note the linear scale of the y-axis as opposed to the logarithmic scale in figure 5c.)

The scale distribution of the ratio of magnetic dissipation to energy is shown in figure 15(b) for different  $t$ . It has already been noted that an isotropic flow satisfies the condition  $\mu(k)/E(k) = 2/3\tau_J^{-1} = \text{const}$ . One can see in figure 15(b) that the magnetic field does not influence the spectrum of Joule dissipation. Except for about 10% fluctuations the ratio  $\mu(k)/E(k)$  is independent of  $k$ . This phenomenon was also observed in the case of large magnetic interaction number (see figure 5d). The peculiarity of the case of a weak magnetic field is that the spectrum is practically independent of time. The root-mean-square of  $\mu(k)/E(k)\tau_J$  was calculated to be equal 0.6623 at  $t = t_0$ , 0.622 at  $t = t_0 + 11.2\tau_J$ , 0.6604 at  $t = t_0 + 26.6\tau_J$ , and 0.6428 at  $t = t_0 + 42\tau_J$ . All the values are close to  $2/3$  corresponding to isotropic flow. Thus, we can consider the spectra in figure 15(b) as one more demonstration of retention of (at least approximate) isotropy of the flow.

## 6. Intermediate magnetic interaction parameter

We have shown above that the flow evolution depends strongly on the magnetic interaction parameter. At large  $N$  rapid irreversible transition into purely two-dimensional, laminar, steady flow occurs. On the other hand, if  $N$  is small, the flow remains three-dimensional, turbulent, and isotropic. Below we demonstrate the possibility of the third kind of evolution, namely an intermittent behaviour.

To this end, a run with an intermediate initial value of the magnetic interaction parameter  $N(t_0) = 0.4$  was performed. We used the same numerical resolution  $64^3$ , kinematic viscosity  $\nu = 0.08453$ , initial Reynolds number  $Re(t_0) = 128$ , and velocity field at  $t = t_0$  as in the case of a weak magnetic field discussed in the previous section.

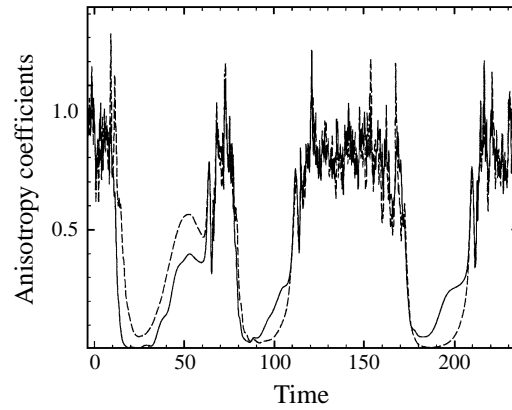


FIGURE 16. Temporal evolution of anisotropy of the intermittent solution at intermediate magnetic interaction parameter  $N_0 = 0.4$ : normalized mean-square velocity gradients  $G_1$  (—) and  $G_2$  (---) (cf. figures 1 and 13a for comparison with the cases of high and low magnetic interaction parameters).

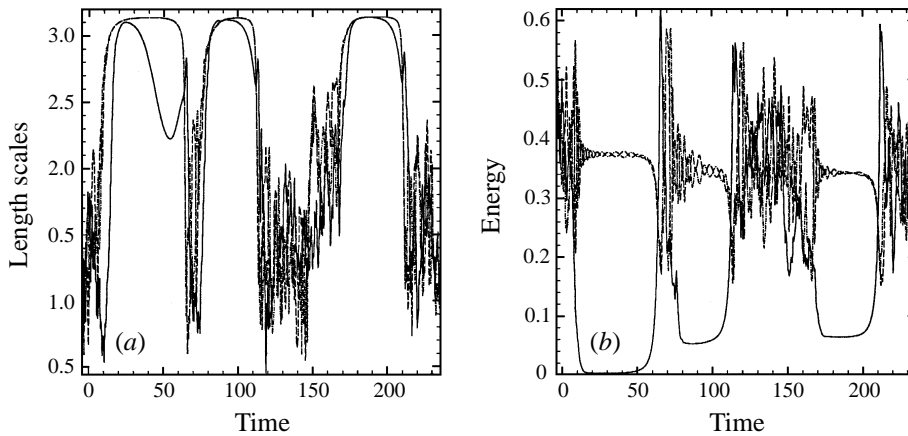


FIGURE 17. Evolution of the integral characteristics of the flow at intermediate magnetic interaction parameter  $N_0 = 0.4$  (cf. figures 2a, b and 13b). (a) Length scales of the flow. —, — —, — · — · —, transverse integral length scales  $L_1$  and  $L_2$ ; — — —, parallel integral length scale  $L_3$ . (b) Total energies of velocity components  $E_1$  (—),  $E_2$  (— · — · —), and  $E_3$  (— — —).

Integral characteristics of the flow are shown in figures 16–18. One can see that they present a typical example of temporal intermittency. Turbulent bursts alternate with periods of quasi-laminar, quasi-two-dimensional behaviour.

The sequence of flow transformations at  $t > t_0$  is the following. After the period of initial development (which is not short since the time unit is now  $2.5\tau_{tu}$ ) the flow undergoes a transition similar to the transition observed at  $N_0 = 10$ . The anisotropy coefficients  $G_1$  and  $G_2$  decrease rapidly, indicating that the flow is getting highly anisotropic. Integral length scales  $L_i$  grow and reach their maximum possible value  $\pi$  hinting at the formation of large-scale structures. The energy  $E_3$  of the vertical velocity component falls to a small but non-zero value. At that time, the transverse velocity components reduce strongly the amplitude of their fluctuations and stabilize at an approximately constant level.

By the analogy with the case  $N_0 = 10$ , all these processes suggest the beginning of transition to a large-scale, quasi-two-dimensional, quasi-laminar flow. The evolution of

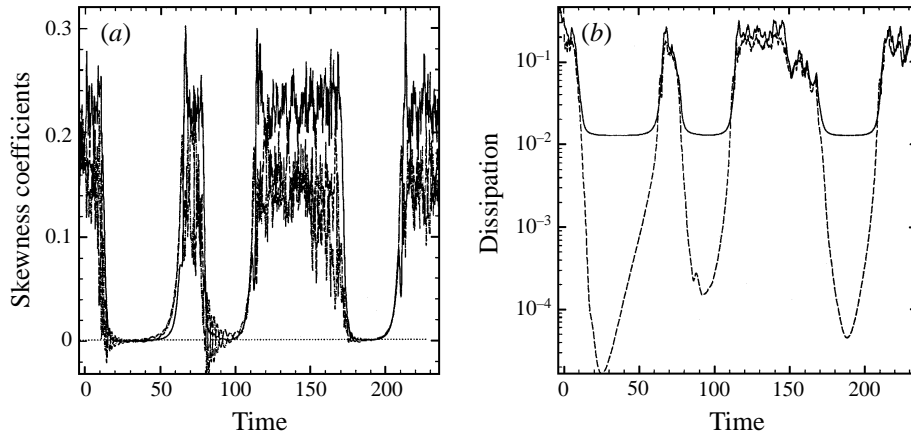


FIGURE 18. Integral characteristics of the flow at  $N_0 = 0.4$  (cf. figure 4*a, b*). (*a*) Skewness coefficients (3.6). —, parallel coefficient ( $S_3$ ); — — — (— · — · —), transverse coefficients  $S_1$  ( $S_2$ ). (*b*) Total viscous ( $\epsilon$  denoted as —) and magnetic ( $\mu$  denoted as — —) dissipation.

skewness coefficients shown in figure 18(*a*) confirms this assumption. The coefficients  $S_i$  fall rapidly and, then, oscillate slightly in such a way that their sum is approximately zero. One more confirmation is in figure 18(*b*) where the total viscous and magnetic dissipations are given. Viscous dissipation decreases to a value which is about ten times smaller than the initial one and, after that, remains constant for a long time. As will be shown below such a behaviour is due to the process of merging the small-scale vortices into large vortical structures and corresponding change of the energy spectrum. The drastic decrease of magnetic dissipation can be explained only by two-dimensionalization of the flow. The last fact is confirmed by the angular energy spectrum below.

The large-scale, quasi-two-dimensional structures developed at the initial stage under the impact of the magnetic field are obviously unstable. What is more, this instability cannot be suppressed by magnetic dissipation. One can see in figures 16–18 that after a certain time, the restoration of three-dimensional turbulent flow occurs. All integral characteristics return to the behaviour typical of the flow without or with a very weak magnetic field. After that, growing magnetic dissipation leads to the repetition of the process of two-dimensionalization and laminarization.

Visualized flow structures typical of different stages of the intermittent flow evolution are shown in figures 19–21. Vorticity vectors  $\boldsymbol{w}$  with the amplitude  $|\boldsymbol{w}| > 2.5w_{mean}$  are drawn in the whole computational box. Figure 19 presents an example of quasi-two-dimensional flow corresponding to ‘laminar’ periods. One can see that the vorticity field strongly resembles the field found in the case  $N_0 = 10$  as a final state (cf. figure 10). Two large counter-rotating columnar vortices determine the flow structure. The vertical vorticity component is dominating, its mean amplitude being six times larger than that of the transverse vorticity components. There is a distinction of the flow in figure 19 from that in figure 10. In the former vortices are twisted. This is obviously the result of inherent instability which cannot be suppressed by the magnetic field at  $N_0 = 0.4$ .

One can see in figure 20 that the instability causes the disintegration of columnar vortices and the formation of vortex structures of a smaller scale. These structures, in turn, break down. After several tens of eddy turnover times  $\tau_{tu}$ , the evolution results in the restoration of three-dimensional highly turbulent flow. An example is given

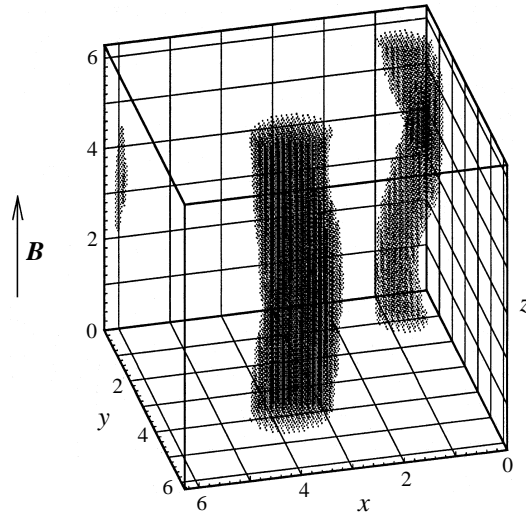


FIGURE 19. An example of quasi-two-dimensional, quasi-laminar structure of temporarily intermittent flow at  $N_0 = 0.4$ : snapshot of vorticity fields at  $t = t_0 + 92\tau_J$  is shown. Vorticity vectors  $\boldsymbol{w}$  with  $|\boldsymbol{w}| > 2.5w_{mean}$  are plotted.

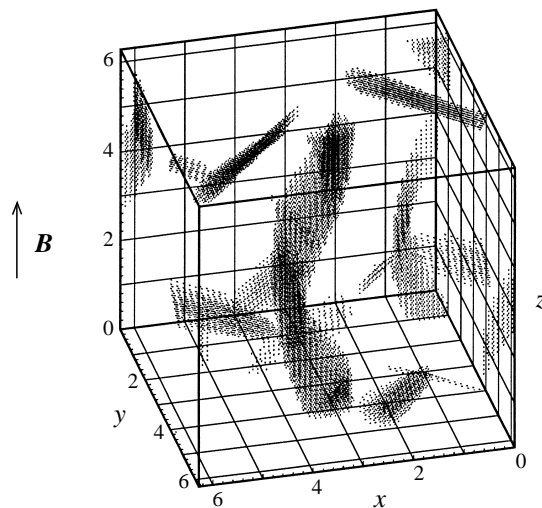


FIGURE 20. Breakdown of the flow in figure 19: vorticity vectors  $\boldsymbol{w}$  with  $|\boldsymbol{w}| > 2.5w_{mean}$  are shown at  $t = t_0 + 110\tau_J$  and  $N_0 = 0.4$ .

in figure 21. The vorticity field consists now of the small-scale structures typical of isotropic turbulence. It can be seen in figures 16–18 that this flow pattern corresponds to intense fluctuations of integral characteristics and the restoration of isotropy.

Wavenumber and angular spectra of flow energy are presented in figure 22(a, b). The spectra corresponding to the flow structure in figure 19 are typical of quasi-two-dimensional, large-scale, quasi-laminar flow. The wavenumber spectrum  $E(k)$  is much steeper than the isotropic one, explaining the sharp decrease of viscous dissipation in figure 18(b). The angular spectrum  $\Phi(\theta)$  reveals a high degree of anisotropy of the flow. The total energy contained in the modes with wavenumber vectors out of

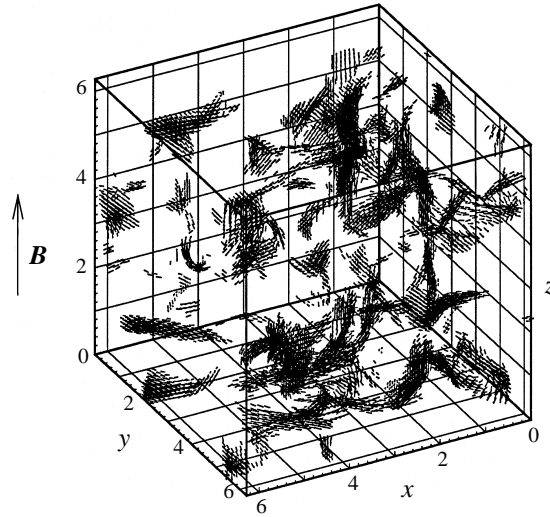


FIGURE 21. An example of three-dimensional turbulent structure of temporarily intermittent flow at  $N_0 = 0.4$ : vorticity vectors  $\boldsymbol{w}$  with  $|\boldsymbol{w}| > 2.5w_{mean}$  at  $t = t_0 + 134\tau_J$  are plotted.

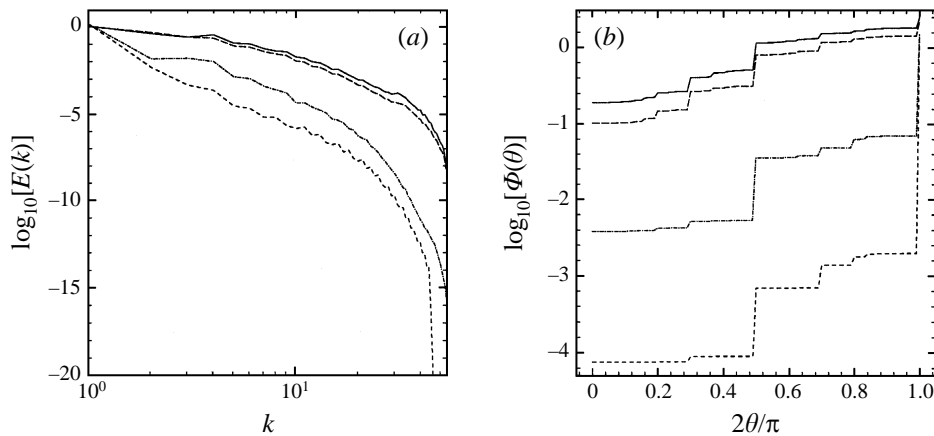


FIGURE 22. Temporal evolution of flow spectra at intermediate magnetic interaction parameter  $N_0 = 0.4$  (cf. figures 5a, 5c and 15a for comparison with the cases of large and small  $N_0$ ): —,  $t = t_0$ ; - - -,  $t = t_0 + 92\tau_J$ ; - · - · - ·,  $t = t_0 + 110\tau_J$ ; — — —,  $t = t_0 + 134\tau_J$ . (a) Energy spectrum  $E(k)$ . (b) Angular energy distribution  $\Phi(\theta) = \int_0^\theta E(\lambda)d\lambda$ , where  $E(\lambda)$  is the angular spectrum of flow energy.

the plane perpendicular to the magnetic field is less than  $2 \times 10^{-3}$ . This angular redistribution of energy is clearly responsible for the decrease of magnetic dissipation.

On the other hand, spectra corresponding to the flow in figure 21 demonstrate a high degree of restoration of isotropic small-scale turbulence as shown in figure 22. Both wavenumber and angular spectra differ only slightly from those for the initial state at  $t = t_0$ .

The flow characteristics in figures 16–18 demonstrate the temporal behaviour which is reminiscent of classical intermittency in dynamical systems with few degrees of freedom. Unfortunately, a detailed analysis of the time series using tools from dynamical system theory was not possible due to their limited length.

The example of the intermittent solution discussed in this section seems to point to the necessity of refinement of the conventional picture of MHD turbulence at an intermediate interaction parameter. This picture is mostly due to Alemany *et al.* (1979). They performed an experimental study of decaying MHD turbulence under a longitudinal external magnetic field at moderate interaction parameters and Reynolds numbers of an order of magnitude larger than in our calculations. The energy spectrum  $E(k) \sim t^{-2}k^{-3}$  found in experiments was explained by the establishment of a quasi-steady equilibrium between the nonlinear angular energy transfer and the Joule dissipation. This equilibrium was supposed to hold over the whole wavenumber range. This explanation can be extended to the  $k^{-3}$  energy spectra measured in duct flows, the latter case being obviously more close to our calculations with forcing.

The picture outlined above implies that a flow with a statistically steady level of anisotropy which is, however, far from being two-dimensional can develop in the case when the magnetic field is not strong enough to create quasi-two-dimensional state. Our calculations demonstrate the possibility of another scenario in this case. The flow has a strongly intermittent history consisting of the transitions between quasi-two-dimensional, quasi-laminar and quasi-isotropic turbulent states. This result does not exclude the existence of statistically steady anisotropic regimes characterized by the balance between Joule dissipation and nonlinear energy transfer. Such states can be found at smaller  $N$ , larger  $Re$  or, what seems to be more probable, in calculations with another type of forcing.

## 7. Concluding remarks

We have studied forced homogeneous turbulence in an electrically conducting fluid subject to a uniform magnetic field. The utilization of the so-called quasi-static approximation, appropriate for low magnetic Reynolds numbers, results in a conceptually simple model which differs from the usual Navier–Stokes equation only by the presence of an additional anisotropic Joule dissipation term and which can be efficiently implemented using pseudospectral techniques.

The present work seems to be one of the first to implement the direct numerical simulation of the long-time evolution of MHD turbulence at low magnetic Reynolds number. Of the previous studies only those of Schumann (1976) and Hossain (1991) are relevant. The difference between our calculations and those of Schumann is that we performed long-run simulations of forced flow at intermediate Reynolds number, whereas Schumann calculated decaying turbulence at smaller Reynolds number using short-time runs with low numerical resolution. Apart from some distinctions due to a different forcing scheme, our calculations with strong magnetic field agree well with the results of Hossain. A novelty of our study is that the Reynolds number is higher and the cases of weak and moderate magnetic field are considered.

The main result of the present work consists of a detailed quantitative characterization of statistically steady MHD turbulence at  $R_m \ll 1$ . In particular, simulations provide unambiguous evidence for the existence of three characteristic types of MHD turbulence corresponding to low, intermediate and high magnetic interaction parameter, respectively.

In the case  $N \ll 1$ , corresponding to a weak magnetic field, we find that the behaviour of MHD turbulence does not significantly differ from ordinary (non-magnetic) turbulence. This result provides a firm justification for the neglect of Joule dissipation in applications involving low magnetic interaction parameter such as

electromagnetic boundary layer control in low-conductivity fluids like sea water (see e.g. Tsinober 1990).

The regime of moderate magnetic field is found to be characterized by a delicate interplay between long-lasting periods of quasi-two-dimensional dynamics and erratic three-dimensional turbulent bursts with a high degree of isotropy. This strongly intermittent behaviour, although being clearly the result of the competition between Joule dissipation and nonlinear energy transfer, is not fully understood yet and is well worth further detailed investigation. In particular, the role of large-scale forcing in the formation of this regime should be carefully studied. The existence of the intermittent regime also has some interesting consequences for the practical question of magnetic damping of turbulence, relevant in various metallurgical applications. Figures 16–22 provide a vivid illustration of the fact that the intuitive picture of the damping influence of a magnetic field may sometimes be misleading. Although the overall damping effect of the magnetic field by Joule dissipation is present, it does not necessarily guarantee a velocity field whose temporal behaviour is smoother than in the non-magnetic case. As a consequence, caution must be exercised when making predictions about the magnetic damping of turbulence in systems with  $N \sim 1$ .

In the case of a strong magnetic field (large magnetic interaction parameter) the flow rapidly becomes two-dimensional. Its evolution at late stages is reproduced by the two-dimensional Navier–Stokes equations independent of the coordinate in the direction of the magnetic field. At  $t \rightarrow \infty$  the solution approaches the purely two-dimensional steady state having the form of cellular Kolmogorov flow. This specific form is certainly due to the boundary conditions and forcing employed in the calculations. We can only assume that these our results model some general properties of real MHD flows. To be consistent with the highly idealized formulation considered in this paper and allow purely two-dimensional flows the experimental setup must include only rigid walls parallel to the magnetic field. Such a setup was proposed by Tsinober (1990). It involves the flow through a channel with annular cross-section and a uniform magnetic field in the azimuthal direction.

Although our numerical resources are insufficient to obtain a regime of two-dimensional turbulence, the simulations permit us to draw a qualitative picture of the behaviour that would be expected if the  $N \gg 1$  calculations were performed with much higher Reynolds number. It is clear that the large-scale structures with scale  $\ell$  would have a two-dimensional turbulent behaviour as long as the magnetic interaction parameter calculated for the typical eddy of size  $\ell$  obeys  $N_\ell \gg 1$ . As soon as the size of the structure has diminished such that  $N_\ell \sim 1$  the eddies would undergo erratic local three-dimensional bursts, similar to the events shown in figures 16–18 in which the energy could then cascade down to the Kolmogorov scale according to the picture of homogeneous turbulence.

It is important to know the limits of validity of the quasi-static approximation. In order to assess them let us consider the full equation

$$\partial_t \mathbf{b} + (\mathbf{u} \cdot \nabla) \mathbf{b} - (\mathbf{b} \cdot \nabla) \mathbf{u} - \eta \Delta \mathbf{b} = (\mathbf{B}_0 \cdot \nabla) \mathbf{u} \quad (7.1)$$

for the magnetic field perturbation. The quasi-static approximation is obtained by dropping the first three terms on the left-hand side. It may appear at first glance that the approximation breaks down once the Joule dissipation has acted long enough to damp significantly the parallel gradients in  $\mathbf{u}$  and, thereby, to reduce the right-hand side of equation (7.1). One could suppose that in this case the terms  $(\mathbf{u} \cdot \nabla) \mathbf{b}$  and  $(\mathbf{b} \cdot \nabla) \mathbf{u}$  become of the same order of magnitude as the right-hand-side term and cannot be

neglected. The simple qualitative answer is that according to the quasi-static solution

$$\mathbf{b} = \eta^{-1} \Delta^{-1} (\mathbf{B}_0 \cdot \nabla) \mathbf{u} = \eta^{-1} B_0 \Delta^{-1} \partial_{\parallel} \mathbf{u} \quad (7.2)$$

(where  $\partial_{\parallel}$  stands for the gradient in the direction of the magnetic field) the fluctuations  $\mathbf{b}$  decrease in proportion to the decrease of the typical parallel gradient  $\partial_{\parallel} \mathbf{u}$ . Therefore, the ratios

$$\frac{(\mathbf{u} \cdot \nabla) \mathbf{b}}{(\mathbf{B}_0 \cdot \nabla) \mathbf{u}} \quad \text{and} \quad \frac{(\mathbf{b} \cdot \nabla) \mathbf{u}}{(\mathbf{B}_0 \cdot \nabla) \mathbf{u}}$$

retain the same order of magnitude as the flow develops towards the quasi-two-dimensional state.

If a two-dimensional state is achieved, the right-hand side being zero, equation (7.1) always has the unique asymptotic solution  $\mathbf{b} = 0$  no matter whether the terms  $(\mathbf{u} \cdot \nabla) \mathbf{b}$  and  $(\mathbf{b} \cdot \nabla) \mathbf{u}$  are neglected or not. This is due to the fact that two-dimensional motion cannot support dynamo action (Moffatt 1978).

For general three-dimensional velocity fields the quasi-static approximation breaks down when the magnetic Reynolds number becomes sufficiently large to allow a dynamo effect. This can happen even for the flow departing only slightly from two-dimensionality. In this case the linear operator on the left-hand side of equation (7.1) will possess exponentially growing solutions which, after sufficiently long time, will supplant the quasi-static solution (7.2). Such behaviour was observed by Weisshaar (1988) for  $P_m = 1$ . In the present case, however, such behaviour is excluded by the assumption  $Re_m \ll 1$ . The value of the critical magnetic Reynolds number can be made more precise for each specific geometry using methods analogous to energy stability theory.

From the practical viewpoint it should be noted that the validity of the quasi-static approximation on the laboratory and industrial scales derives from the fact that dynamo action is irrelevant in these cases.

The forcing used in the present work involves some degree of ambiguity. It would therefore be interesting to remove this deficiency while keeping the convenient framework of homogeneous turbulence. This could for instance be done by adding a temperature field and buoyancy force so that the flow would then be forced by the natural mechanism of Rayleigh–Bénard instability rather than artificially. (For a study of effect of an external magnetic field on Rayleigh–Bénard convection see e.g. Meneguzzi *et al.* 1987.)

The problem of Rayleigh–Bénard convection in the presence of a magnetic field can also be of interest for the understanding of astro- and geophysical systems including buoyancy as well as Lorentz forces. The quasi-static approximation based on the limit of low magnetic Reynolds number is not applicable to such systems. However, if one studies the motions at small scales, the local magnetic Reynolds number can be considered as a small parameter and our results are valid at this scale, at least qualitatively. Evidence for this can be found, e.g., in direct numerical simulations of decaying MHD turbulence by Oughton *et al.* (1994), where the full MHD equations including the non-steady perturbation  $\mathbf{b}$  of the imposed magnetic field  $\mathbf{B}_0$  were solved. A sufficiently strong magnetic field was found to suppress turbulent fluctuations in its direction and cause the development of anisotropy in an initially isotropic flow. The modes with the wavenumber vectors perpendicular to  $\mathbf{B}_0$  accumulate most of the flow energy. It was also shown that the anisotropy is more pronounced at small scales, which is, clearly, in correspondence with above assumption of applicability of our results at such scales. The qualitative similarity of the statistical properties of the velocity field between the

work of Oughton *et al.* (1994) and the present study is especially surprising in view of the fact that the former simulations have been carried out for large magnetic Reynolds number and magnetic Prandtl number  $P_m = 1$ , whereas ours is for  $Re_m \ll 1$  and  $P_m \ll 1$ .

The authors thank A. Tsinober, Yu. Kolesnikov, P. Davidson, and J. Sommeria for interesting discussions and useful comments. This work was supported by the Deutsche Forschungsgemeinschaft under Grant INK 18/A1-1 (Innovationskolleg Magnetofluidodynamik). The computations have been performed at the CRAY-M94 and CRAY-T90 at the Höchstleistungsrechenzentrum Jülich, Germany.

**Appendix. Linear and energy stability analysis of two-dimensional cellular flow**

We perform stability analysis of the two-dimensional flow

$$V = \begin{cases} b \sin y \\ a \sin x \\ c \cos x - bc/a \cos y, \end{cases} \tag{A 1}$$

where  $a$ ,  $b$ , and  $c$  are arbitrary constants satisfying

$$a^2 + b^2 + c^2(1 + b^2/a^2) = 4E_0. \tag{A 2}$$

The flow is an exact solution of the Navier–Stokes and incompressibility equations (2.1), (2.2) with forcing. Being independent of the coordinate  $z$  in the direction of the magnetic field the flow is not affected by the Joule dissipation. Arbitrary three-dimensional perturbations  $\mathbf{u}$ ,  $p$  satisfying the incompressibility condition are imposed on the basic flow (A 1). We suppose that the perturbations are spatially periodic with the period  $2\pi$  in each direction. It is supposed also that the energy supplied by forcing is consumed fully by the process of maintaining the basic flow. Therefore, the forcing term does not appear in the following perturbation equations:

$$\frac{\partial}{\partial t} \mathbf{u} + (\mathbf{u} \cdot \nabla) V + (V \cdot \nabla) \mathbf{u} + (\mathbf{u} \cdot \nabla) \mathbf{u} = -\frac{1}{\rho} \nabla p + \nu \Delta \mathbf{u} - \tau_J^{-1} \Delta^{-1} \frac{\partial^2 \mathbf{u}}{\partial z^2}, \tag{A 3}$$

$$\nabla \cdot \mathbf{u} = 0, \tag{A 4}$$

where  $\tau_J^{-1} = \sigma B_0^2 / \rho$  is reciprocal Joule time.

As a first step we perform a linear stability analysis, i.e. term  $(\mathbf{u} \cdot \nabla) \mathbf{u}$  is neglected in (A 3). We consider the case of a one-dimensional basic flow with  $b = 0$ . It will be shown that in this case all periodic solutions of linearized equations decay at any  $\nu$  and  $\tau_J$ . The equations (A 3), (A 4) transform into

$$\left. \begin{aligned} \frac{\partial u}{\partial t} + a \sin x \frac{\partial u}{\partial y} + c \cos x \frac{\partial u}{\partial z} &= -\frac{1}{\rho} \frac{\partial p}{\partial x} + \nu \Delta u - \tau_J^{-1} \Delta^{-1} \frac{\partial^2 u}{\partial z^2}, \\ \frac{\partial v}{\partial t} + a \cos x u + a \sin x \frac{\partial v}{\partial y} + c \cos x \frac{\partial v}{\partial z} &= -\frac{1}{\rho} \frac{\partial p}{\partial y} + \nu \Delta v - \tau_J^{-1} \Delta^{-1} \frac{\partial^2 v}{\partial z^2}, \\ \frac{\partial w}{\partial t} - c \sin x u + a \sin x \frac{\partial w}{\partial y} + c \cos x \frac{\partial w}{\partial z} &= -\frac{1}{\rho} \frac{\partial p}{\partial z} + \nu \Delta w - \tau_J^{-1} \Delta^{-1} \frac{\partial^2 w}{\partial z^2}, \end{aligned} \right\} \tag{A 5}$$

$$\frac{\partial u}{\partial x} + \frac{\partial v}{\partial y} + \frac{\partial w}{\partial z} = 0, \tag{A 6}$$

where  $\mathbf{u} = (u, v, w)$ . The system coefficients depend now on  $x$  only. Taking into account the periodic boundary conditions we can use the Fourier expansion

$$(u, v, w, p)(x, y, z, t) = e^{\sigma t + i(my + nz)} \sum_{l=-\infty}^{\infty} (u_l, v_l, w_l, p_l) e^{ilx}, \quad (\text{A } 7)$$

where  $m$  and  $n$  are arbitrary integer wavenumbers and  $\sigma$  is the complex growth rate. After substituting (A 7) into (A 5) and taking the divergence we obtain the expression for pressure coefficients

$$p_l = \frac{\rho}{k^2} [u_{l-1}(ima - cn) + u_{l+1}(ima + cn)], \quad (\text{A } 8)$$

where  $k^2 = l^2 + m^2 + n^2$ . Using (A 8) the first equation in (A 5) can be reduced to the equation for the  $u$ -component only. After simple transformations one obtains

$$\begin{aligned} (\alpha^2 + l^2) \left[ \sigma + v(\alpha^2 + l^2) + \tau_J^{-1} \frac{n^2}{\alpha^2 + l^2} \right] u_l + \frac{am + icn}{2} [\alpha^2 - 1 + (l-1)^2] u_{l-1} \\ - \frac{am - icn}{2} [\alpha^2 - 1 + (l+1)^2] u_{l+1} = 0, \end{aligned} \quad (\text{A } 9)$$

where  $\alpha^2 = n^2 + m^2$ .

Now we introduce new variables  $s_l$  such that

$$u_l = Q e^{i\phi} s_l,$$

where  $Q$  and  $\phi$  are the amplitude and the phase of the complex constant  $(am + icn)/2$ . For  $s_l$  we can write the final equation

$$\begin{aligned} Q^{-1}(\alpha^2 + l^2) \left[ \sigma + v(\alpha^2 + l^2) + \tau_J^{-1} \frac{n^2}{\alpha^2 + l^2} \right] s_l \\ + [\alpha^2 - 1 + (l-1)^2] s_{l-1} - [\alpha^2 - 1 + (l+1)^2] s_{l+1} = 0. \end{aligned} \quad (\text{A } 10)$$

Equation (A 10) is similar to equation (1.4) in Meshalkin & Sinai (1961). The only differences are that the positive constant coefficient  $Q^{-1}$  has a different expression and the additional magnetic dissipation term  $\tau_J^{-1} n^2 / (\alpha^2 + l^2)$  appears in our case. Meshalkin & Sinai have found that at  $\alpha > 1$  real part of the growth rate  $\sigma$  is always negative, that is, the basic flow is unconditionally stable. From their solution one can see that the value of  $Q^{-1}$  does not affect this conclusion. It is also clear that the magnetic dissipation term cannot cause any instability. Therefore, the result of Meshalkin & Sinai is valid for equation (A 10) also. Three-dimensional perturbations have  $\alpha > \sqrt{2}$ . Therefore, we can state that basic solution (A 1) with  $b = 0$  is linearly stable at any  $v$  and  $\tau_J$  to any three-dimensional perturbations having  $2\pi$ -periodicity in each direction.

The linear analysis above has shown that between the basic solutions (A 1) there are unconditionally stable ones. In an attempt to obtain more comprehensive information we solve below the energy stability problem. Once again, periodic three-dimensional perturbations are considered but now we look for the conditions for an arbitrary finite-amplitude solution of (A 3), (A 4) to decay. The usual energy stability method is applied (see e.g. Straughan 1992). Energy stability equations can be given as

$$v_E \Delta \mathbf{u} - \tau_J^{-1} \Delta^{-1} \frac{\partial^2 \mathbf{u}}{\partial z^2} - \mathbf{D} \cdot \mathbf{u} = -\nabla \pi, \quad (\text{A } 11)$$

$$\nabla \cdot \mathbf{u} = 0, \quad (\text{A } 12)$$

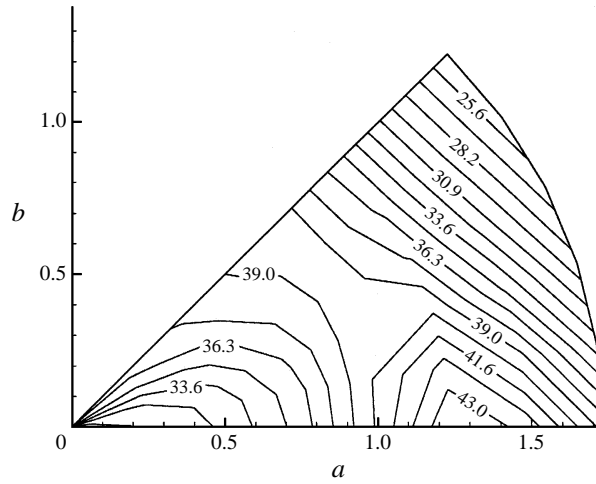


FIGURE 23. Contours of energy stability limit  $v_E$  of the square periodic flow (A 1) as a function of constants  $a$  and  $b$  at  $\tau_J^{-1} = 4.0$ .

where

$$D_{ij} = \frac{1}{2} \left( \frac{\partial V_i}{\partial x_j} + \frac{\partial V_j}{\partial x_i} \right)$$

is the symmetric part of the gradient tensor of the basic velocity field and  $\pi(\mathbf{x})$  is a Lagrange multiplier. The variational derivation of (A 11), (A 12) is the same as that for the Navier–Stokes system (Straughan 1992). The only difference is that magnetic dissipation leading to the extra term in (A 11) should be taken into account.

The energy stability limit  $v_E$  is defined as an eigenvalue of the problem consisting of (A 11), (A 12) and periodic boundary conditions. The meaning of this limit is that, at  $v > v_E$ , the total energy  $E(t) = \frac{1}{2} \langle u^2 + v^2 + w^2 \rangle$  of an arbitrary perturbation to the basic flow (A 1) decays exponentially with time.

We solve the eigenvalue problem numerically using the Fourier expansion

$$(u, v, w, \pi)(x, y, z) = e^{inz} \sum_{l,m=-M}^M (u_{lm}, v_{lm}, w_{lm}, \pi_{lm}) e^{i(lx+my)}, \quad (\text{A } 13)$$

where  $M$  is the numerical resolution and the vertical wavenumber  $n$  can take an arbitrary integer value. After substituting (A 13) into (A 11), (A 12) and performing simple transformations one obtains an algebraic eigenvalue problem for a matrix of the order  $3(2M+1)^2$ . This problem is solved numerically for different  $n$  and basic flow parameters  $a$ ,  $b$ , and  $c$ . Since the stability to arbitrary perturbation is tested, critical  $v_E$  must be minimized over  $n$ . We considered only three-dimensional perturbations with  $n \neq 0$  and have found that the modes with  $n = 1$  are always most dangerous. The stability limit  $v_E$  must be also maximized over  $a$ ,  $b$ , and  $c$  to find the most stable configuration of the basic flow. Symmetry properties of the problem allow the region (A 2) of parameters under consideration to be reduced to:

$$0 \leq a \leq 2E_0^{1/2}, \quad 0 \leq b \leq \min[a; (4E_0 - a^2)^{1/2}], \quad c = \left( \frac{4E_0 - a^2 - b^2}{1 + b^2/a^2} \right)^{1/2}.$$

As an example of calculations, contours of constant  $v_E$  on the  $(a, b)$ -plane are

shown in figure 23 for the case  $\tau_J^{-1} = 4$ . The computations are performed with the resolution  $M = 5$ . One can see the dependence of  $v_E$  on the basic flow configuration. It was found that at  $\tau_J^{-1} < 0.5$  the most stable basic flow has  $U = V = 0$  and  $W = (2E_0)^{1/2}(\cos x + \cos y)$ .

At  $\tau_J^{-1} > 0.5$  the most stable configuration is with  $b = 0$ . This provides the possibility of solving the eigenvalue problem (A 11), (A 12) much more accurately. The coefficients of the equations depend only on  $x$  in this case and one-dimensional Fourier expansion can be used instead of (A 13).

## REFERENCES

- ALEMANY, A., MOREAU, R., SULEM, P. L. & FRISCH, U. 1979 Influence of an external magnetic field on homogeneous MHD turbulence. *J. Méc.* **18**, 277–313.
- BORUE, V. 1993 Spectral exponents of enstrophy cascade in stationary two-dimensional homogeneous turbulence. *Phys. Rev. Lett.* **71**, 3967–3970.
- BRANOVER, H. 1978 *Magnetohydrodynamic Flows in Ducts*. Halsted.
- CAMBON, C., MANSOUR, N. N. & GODEFERD, F. S. 1997 Energy transfer in rotating turbulence. *J. Fluid Mech.* **337**, 303–332.
- CUEVAS, S., PICOLOGLOU, B. F., WALKER, J. S., TALMAGE, G. & HUA, T. Q. 1997a Heat transfer in laminar and turbulent liquid-metal MHD flows in square ducts with thin conducting or insulating walls. *Intl J. Engng Sci.* (to appear).
- CUEVAS, S., PICOLOGLOU, B. F., WALKER, J. S., TALMAGE, G. & HUA, T. Q. 1997b Liquid-metal MHD flow in rectangular ducts with thin conducting or insulating walls: laminar and turbulent solutions. *Intl J. Engng Sci.* (to appear).
- CUEVAS, S., RAMOS, E. & PICOLOGLOU, B. F. 1996 Turbulent liquid-metal flow in rectangular ducts with thin conducting walls and strong magnetic fields. Presented at *VIII Beer-Sheva Seminar*.
- DAVIDSON, P. A. 1995 Magnetic damping of jets and vortices. *J. Fluid Mech.* **299**, 153–186.
- DAVIDSON, P. A. 1997 The role of angular momentum in the magnetic damping of turbulence. *J. Fluid Mech.* **336**, 123–150.
- ECKERT, S. 1997 Experimentelle Untersuchung turbulenter Flüssigmetall- und Flüssigmetall-Gas-Strömungen in einem äusseren Magnetfeld. PhD thesis, TU Dresden, Dresden.
- GELFGAT, Y. M., LIELAUSIS, O. A. & SHCHERBININ, E. V. 1975 *Liquid Metal under the Influence of Electromagnetic Forces*. Zinatne (in Russian).
- GOTOH, K. & YAMADA, M. 1986 The instability of rhombic cell flow. *Fluid Dyn. Res.* N1, 165–176.
- HINZE, J. O. 1959 *Turbulence*. McGraw-Hill.
- HOSSAIN, M. 1991 Inverse energy cascades in three-dimensional turbulence. *Phys. Fluids B* **3**, 511–514.
- HOSSAIN, M. 1994 Reduction in the dimensionality of turbulence due to a strong rotation. *Phys. Fluids* **6**, 1077–1080.
- JIMENEZ, J., WRAY, A. A., SAFFMAN, P. G. & ROGALLO, R. S. 1993 The structure of intense vorticity in isotropic turbulence. *J. Fluid Mech.* **255**, 65–90.
- KOLESNIKOV, YU. B. & TSINOBER, A. B. 1974 Experimental study of two-dimensional grid turbulence. *Izv. AN SSSR. Mekh. Zhidk. i Gaza* **4**, 146.
- KRAICHNAN, R. H. 1967 Inertial ranges in two-dimensional turbulence. *Phys. Fluids* **10**, 1417–1423.
- MATTHAEUS, W. H., STRIBLING, W. T., MARTINEZ, D. & OUGHTON, S. 1991 Selective decay and coherent vortices in two-dimensional incompressible turbulence. *Phys. Rev. Lett.* **66**, 2731–2734.
- MENEGUZZI, M., SULEM, C., SULEM, P. L. & THUAL, O. 1987 Three-dimensional numerical simulation of convection in low-Prandtl number fluids. *J. Fluid Mech.* **182**, 169–191.
- MESHALKIN, L. D. & SINAI, YA. G. 1961 Investigation of the stability of a stationary solution of equations for the plane movement of an incompressible viscous fluid. *J. Appl. Math. Mech. (Prikl. Mat. Mekh.)* **25**, 1140–1143.
- MOFFATT, H. K. 1967 On the suppression of turbulence by a uniform magnetic field. *J. Fluid Mech.* **23**, N3, 571–592.

- MOFFATT, H. K. 1978 *Magnetic Field Generation in Electrically Conducting Fluids*. Cambridge University Press.
- MONTGOMERY, D., MATTHAEUS, W. H., STRIBLING, W. T., MARTINEZ, D. & OUGHTON, S. 1992 Relaxation in two dimensions and the “sinh-Poisson” equation. *Phys. Fluids A* **4**, 3–6.
- MOREAU, R. 1990 *Magnetohydrodynamics*. Kluwer.
- ORSZAG, S. A. 1972 Comparison of pseudospectral and spectral approximation. *Stud. Appl. Maths* **51**, 253.
- OUGHTON, S., PRIEST, E. R. & MATTHAEUS, W. H. 1994 The influence of a mean magnetic field on three-dimensional magnetohydrodynamic turbulence. *J. Fluid Mech.* **280**, 95–117.
- ROBERT, R. & SOMMERIA, J. 1991 Statistical equilibrium states for two-dimensional flows. *J. Fluid Mech.* **229**, 291.
- ROBERTS, P. H. 1967 *An Introduction to Magnetohydrodynamics*. American Elsevier.
- SCHUMANN, U. 1976 Numerical simulation of the transition from three- to two-dimensional turbulence under a uniform magnetic field. *J. Fluid Mech.* **74**, 31–58.
- SHIMOMURA, YU. 1991 Large eddy simulation of magnetohydrodynamic turbulent channel flows under a uniform magnetic field. *Phys. Fluids A* **3**, 3098–3106.
- SOMMERIA, J. & MOREAU, R. 1982 Why, how, and when, MHD turbulence becomes two-dimensional. *J. Fluid Mech.* **118**, 507–518.
- STAQUET, C. & SOMMERIA, J. 1996 Internal waves, turbulence and mixing in stratified flows: a report on Euromech Colloquium 339. *J. Fluid Mech.* **314**, 349–371.
- STRAUGHAN, B. 1992 *The Energy Method, Stability, and Nonlinear Convection*. Springer.
- THESS, A. 1992 Instabilities in two-dimensional spatially periodic flows. Part II: Square eddy lattice. *Phys. Fluids A* **4**, 1396–1407.
- TSINOBER, A. 1990 MHD flow drag reduction. In *Viscous Drag Reduction in Boundary Layers* (ed. D. M. Bushnell & J. N. Hefner). AIAA Prog. Astron. Aeron. Series.
- VINCENT, A. & MENEGUZZI, M. 1991 The spatial structure and statistical properties of homogeneous turbulence. *J. Fluid Mech.* **225**, 1–20.
- VOTSISH, A. D. & KOLESNIKOV, YU. B. 1976a Spatial correlations and vorticity in two-dimensional homogeneous turbulence. *Magn. Gidrodin.* **3**, 25–28.
- VOTSISH, A. D. & KOLESNIKOV, YU. B. 1976b Investigation of transition from three-dimensional turbulence to two-dimensional under a magnetic field. *Magn. Gidrodin.* **3**, 141–142.
- WEISSHAAR, E. 1988 Nonlinear Alfvénic fluctuations in uniform magnetic background fields. *Geophys. Astrophys. Fluid Dyn.* **41**, 141.